Response to reviewer #1

We thank reviewer #1 for careful reading our manuscript and for the positive feedback as well as constructive comments on our work. Below we address first the general and then the minor comments. The reviewer's comments are in **blue**, our responses are in **black** and any additions to the manuscript are in **red**

General comment 1

The manuscript is relatively technical and method oriented. For non-experts within the field it can be hard to understand the possibilities and limitations with the described methods. I suggest that you add more discussion about the possibilities and limitations with the described methods in the summary and conclusion section. One limitation which I think should be discussed a bit more is the uncertainties in the observations. On line 265-266 you write that you assume a 1 % uncertainty in the measured evaporation factor (EF), I think this uncertainty can be substantially bigger. How sensitive is the optimization of all parameter values to the uncertainties in the observations? I.e. what happen if the uncertainty of the measured EF is 5 %?

Response

The question of uncertainties and their influence to the method is an interesting one. In real evaporation measurements the error may be larger than 1%. As the uncertainties vary with experimental setting and may sometimes be challenging to estimate, we concentrated here on the performance of the method in an idealized case.

In addition, we also tested the methods with data set where random noise was introduced to the EF and time. On average the EF error was 1% and ± 10 min in time for long residence time (time > 10 min data points) points. For short residence time data points (time < 10 min data points) the random error in time was 9%. For the 10 minute data point the relative error in time was +77% / -63%. The results of fitting the LLEVAP model with both schemes showed similar results as the data set with no uncertainty in the particle radius / EF and hence we decided not to include it in the manuscript. The results of this new data set are summarized in Table 1.

Table 1: Estimated parameter distributions and correct values for an artificial data set where random noise was introduced to the data set.

Variable	Correct values	MCMC	MCGA (Gaussian)	MCGA (uniform)
$C_{sat,1}$ ($\mu g\ m^{-3}$)	0.01	0.008 – 0.016	0.007 – 0.02	0.006 – 0.014
$C_{sat,2}$ ($\mu g\ m^{-3}$)	1	0.86 – 1.44	0.78 – 1.86	0.79 – 1.37
$C_{sat,3}$ ($\mu g\ m^{-3}$)	1000	567 – 2488	588 – 1530	309 – 6708
$x_{mole,1}$	0.5	0.48 – 0.53	0.49 – 0.56	0.48 – 0.53
$x_{mole,2}$	0.4	0.38 – 0.43	0.35 – 0.42	0.38 – 0.43
$x_{mole,3}$	0.1	0.06 – 0.12	0.07 – 0.11	0.07 – 0.11

General comment 2

Now you use the term "correct" values when you talk about measured and/or literature data on particle phase density, individual compound saturation concentrations and viscosity. But can we really state that we know the correct values of all these parameters? I would avoid using the term

Response

We have replaced the mentions of correct values to literature values when referring to literature values. We are now using the term correct value only when referring to the artificial data sets or the mass / mole fractions in mixtures 1-4 where the estimated parameters have "correct" values in the sense that they are measured or used as an input to a process model to produce the artificial data.

General comment 3

It would also be good to add a short discussion about how the described methods can be used in order to suggest/design new experiments which can give better constrains on the volatility and viscosity properties of SOA particles. Recommendation of new experiments is always welcomed by experimental aerosol scientists.

Response

We have added following discussion on this at the end of conclusions.

Based on the analysis shown here, various parameters can be obtained from experimental data using this method and the design of the experiments can be used to focus experiments on properties of interest. For instance, in order to distinguish between saturation concentrations of low-volatile compounds, small particles and hours long evaporation times are required. On the contrary, to distinguish between semivolatile or intermediate volatility compounds, larger particles and/or high sampling time resolution for the short evaporation time scales are needed.

Minor comment 1

When I read section 3, L250-285 I start to wonder what artificial parameter values of C* and the mole fractions did you actually use in dataset 1-4? Then later when you start to describe the results it become clear to me that these values can be found in figure 2-5. Still, I think it would be good to have a table which provide these values already in Sect. 3. In this table you can also include the best optimization values for these parameters and the 10 th and 90 th percentiles. With this table include you do actually not need all the figures.

Response

We thank Reviewer #1 for this suggestion. We have added new Table 3 which shows the correct values for x_{mole} and C_{sat} for artificial data set 1-4. The old Table 3, Table 4 and Table 5 are now Table 4, Table 5 and Table 6, respectively.

Minor comment 2

In Table 1 and Table 4 some field are empty, but I guess it should be saying e.g. Xmole,dry(t=0 s) "Fitted(min: 0.01 max:1)" and T(K) 293 in all fields. I suggest that you write out explicitly in each column these values, even if they are the same in all experiments/simulations.

Response

Thank you for pointing this out. We have changed Table 1 and Table 4 to explicitly show what these parameters are for each data set or mixture

Minor comment 3

L424-425: You use the term "non-viscous" and "viscous" when talking about mixtures with low-viscosity and high-viscosity. I would recommend that you use the late terms instead and possible specify that the particle-phase mass transfer limitation was negligible in the low-viscosity mixture and hence neglected

Response

We agree with reviewer that using the term "non-viscous" is misleading as every particle has some viscosity. We have changed the text so that non-viscous was changed to "low viscosity" and viscous to "high viscosity". We have also added an explanation of these terms to Sect. 5, line 440 in the revised version.

In the following discussion, "low viscosity" refers to particles where particle phase diffusivity is fast enough so that it doesn't pose a limitation to the evaporation of the volatile compounds and "high viscosity" refers to particles where the particle phase diffusivity is low enough to affect the particles' evaporation rate.

Response to reviewer #2

We thank reviewer #2 for reviewing our manuscript and providing valuable feedback on our work. Below we address first the general and then the specific comments. The reviewer's comments are in blue, our responses are in **black** and any additions to the manuscript are in red

General comment 1

It is noteworthy that the authors do not use numerical values of their measure of model result-data correlation (fitness) for their argumentation. The performance of an optimization algorithm should also be evaluated in terms of how quickly (or how reliably) it reaches a certain threshold of model result-data correlation that justifies consideration of the optimized parameter set (e.g. model result-data residue is comparable to the noise in the experimental data). The authors denote the spread in fitted parameters, but it would also be interesting to see spreads in their measure for correlation, especially in section 3 where two methods are compared.

Response

We considered comparing the model result-data correlation, but decided not to include those because of the methodological differences between the MCGA and Bayesian inference. The main problem we encountered in comparing the two methods was that the Bayesian analysis fundamentally assumes that the estimated parameters have distributions whereas the MCGA algorithm looks for an optimal value which fits the data. This Bayesian vs. frequentist conflict presents challenges when the two methods are compared.

Considering only a situation where one parameter would be optimized, the MCMC algorithm would sample from the posterior distribution of this parameter such that sometimes during the execution also values that fits less well to the experimental data are visited but less often than those parameter values that produce a better fit to the data. For this reason we feel that it would not be fair to compare how the model result-data correlation evolves during the MCMC calculations. This comparison would show that in the MCMC algorithm the model result-data residue sometimes spikes whereas MCGA algorithm consistently moves toward lower residues.

We believe that the best way to compare the algorithms is to think that over multiple optimization rounds the MCGA algorithm also produces a distribution of parameter values which can be compared to the posterior distribution calculated with the MCMC algorithm.

We have clarified our reasoning that led us to only show the parameter estimate distribution in the manuscript by adding the following to Sect. 3 line 276 in the revised version.

The Bayesian inference and the MCMC algorithm assume estimated parameters are random variables with probability distributions, whereas the MCGA algorithm tries to find a single set of input parameters that best fit to the observations. The MCMC algorithm explores the posterior distribution by randomly drawing samples from it. The samples are drawn such that the parameter values that better fit to the data and thus are more probable are drawn more often than the lower probability parameter values that produce worse fits. Because of this fundamental difference between these two approaches, it would not be appropriate to compare how the model output-data residuals evolve during the execution of both algorithms and only the distributions of parameter

estimates from MCMC and MCGA over multiple optimization rounds are used to compare the two methods.

General comment 2

What is the reason to choose MCGA over Bayesian inference for further analysis in this manuscript? Did one method outperform the other in any regard or was it just easier to operate?

Response

As shown in Sect. 3 both methods produce similar distributions for the estimated parameters and there is no obvious evidence that one method is better than the other. We feel that once this comparison is made the choice is up to the person performing the optimization, as rigorous model optimization needs hands-on expertise with the selected method. MCGA was selected for further comparison because we had more experience with Genetic Algorithms as our group has used GA before in Yli-Juuti et al., (2017) and the MCGA method in Buchholz et al., (2019).

General comment 3

I wonder how big the error is that is introduced by combination of the topmost bulk layers in the KM-GAP model during evaporation. This practice in conjunction with discrete layers can introduce step-profiles in evaporation, where evaporation slows down as volatile constituents are depleted from the topmost bulk layer and picks up pace again as soon as layers are merged (and hence volatile component is mixed into the topmost bulk layer). Kinetic models operating with fixed layer sizes and merging schemes have to have mechanisms in place that prevent these artifacts from happening, especially when input parameter optimization is automatized and hence numerical convergence not always manually checked for each combination of input parameters. Which mechanisms are in place in this study to prevent this?

Response

Reviewer #2 raises an important point here. After each KM-GAP simulation we did not check numerically whether the model output contained step-profiles. An efficient method to remove these step-profiles caused by high viscosity in the topmost layer is to increase the number of layers in the model, which decreases the thickness of the topmost layer and leads to layers being merged more frequently, i.e. in practice before all of the volatile component (glycerol in mixtures 3 and 4) is gone from the topmost layer. Based on a random search of the parameter space, large step-profiles are rare in our system but do exist with some combination of the allowed input parameters. However, increasing the number of layers from 30 to e.g. 100 led more often to situations where the diffusion fluxes are too high compared to the amount of molecules in a layer, which in turn resulted in the ODE solver to stop integration as the required time step to solve the molecular transport became too short.

In figure 1 we compare KM-GAP output using the parameter estimates calculated by optimizing to low RH evaporation data of mixtures 3 and 4 with original number of layers (30) and with 100 layers. With both mixtures we see small deviation between the outputs. However, this variation is small compared to the variation in the experimental data.

To check that this numerical problem does not cause a systematic deviation to optimized parameter values, we tested how the best parameter estimates for mixture 3 would change if the candidates in the last generation of an optimization round were rerun with 300 layers (instead of the original 30 layers). The best mole fraction estimates would change by 0.001, C_{sat} estimates would stay the same, $b_{sucrose}$ would change from $10^{12.0}$ to $10^{11.4}$ and $b_{glycerol}$ from $10^{-3.88}$ to $10^{-3.33}$. Based on this analysis, not checking the convergence might have caused the $b_{sucrose}$ estimates to be slightly lower and $b_{glycerol}$ estimates slightly higher. However, the deviations in the estimated b_i parameters are small and do not affect our conclusions.
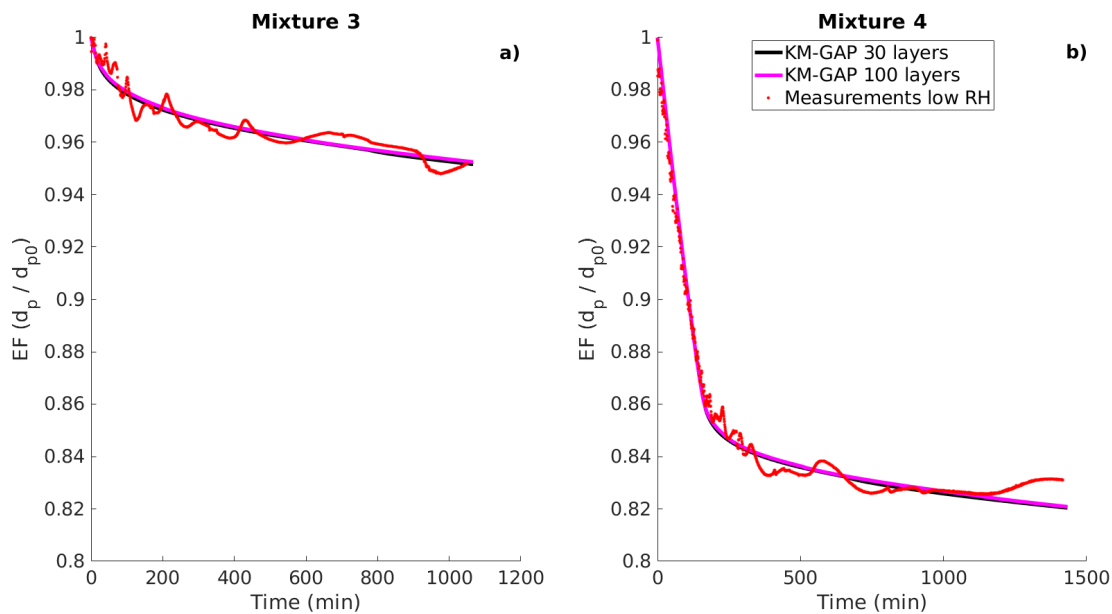

Figure 1: Low RH measurements and KM-GAP output calculated with a set of estimated parameters (C_{sat}, x_{mole} and b_i) and with 30 layers (black solid line) or 100 layers (magenta solid line). a) Low RH measurement data and parameter estimates of mixture 3 in the manuscript. b) Low RH measurement data and parameter estimates of mixture 4 in the manuscript

General comment 4

A stylistic suggestion: A concept that is usually used when talking about model parameter optimization is that of a parameter's (local) sensitivity. Talking about conditions under which model output is sensitive to the numerical value of an input parameter could simplify the (sometimes a little slow-moving) discussion in this manuscript considerably. However, usage of this concept is left to judgment of the authors.

Response

We have elected not to change the discussion as we deal with data sets that can be said to have "correct" answers in terms of literature values or input values used in calculating the artificial data sets. We feel that talking about the distribution of estimates we get from independent optimization runs fits better to the context of our work instead of parameter sensitivity.

Specific comment 1

Sect. 1, l. 45 – What do you mean by "increasing attention has also been given to modeling the particle dynamics to better understand the measurements"? Particle dynamics could refer to processes like deposition and coagulation, but probably means evaporation dynamics here, please clarify.

Response

We have modified the text on line 45 to the following

In addition to experimental methods, increasing attention has also been given to modeling the evaporation process to better understand the measurements

Specific comment 2

Sect. 1, l. 50 – The literature review on kinetic parameter determination through inverse modelling seems a little sparse here. Even in aerosol research, there have been more studies detailing such procedures. Examples include Berkemeier et al. (2016), who determined both diffusion coefficients and reaction rates by inverse modelling or Lowe et al. (2016), who used a Monte Carlo Markov Chain (MCMC) algorithm on artificial data as a tool for sensitivity analysis.

Response

We thank Reviewer #2 for pointing out these excellent publications that we hadn't referred to in our manuscript. We have added references to both of these articles starting from line 51 reading:

Berkemeier et al., (2016) derived kinetic parameters influencing ozone uptake of shikimic acid by fitting to multiple measurements of ozone uptake by the acid at different relative humidities. Lowe et al., (2016) studied the sensitivity of various parameters of Köhler theory by studying the goodness-of-fit to artificial cloud condensation nucleus spectra. ~~The same approach was also used~~ Yli-Juuti et al. (2017) ~~to~~ inferred ...

Specific comment 3

Sect. 2.2, l. 132 – It is counterintuitive to talk about a good candidate having low fitness here since in the biological sense a high fitness would be considered better. "Fitness" is thus usually defined as the inverse of least-squares deviation.

Response

We have changed the manuscript so that when we talk about high fitness we mean an inverse of the mean squared error and thus a good fit candidate now has a higher fitness than a candidate with higher mean squared error. We have also modified the explanation starting from the line 133 in the revised version to the following:

Below, the fitness of a candidate is determined as the inverse of its goodness of fit statistic. The goodness of fit in this work is calculated as a mean squared error (MSE) between the evaporation simulation produced with the candidate's parameter set and the measured evaporation. A lower value for goodness of fit statistic, i.e. lower MSE, means higher value for fitness and a better candidate.

Sect. 2.2, l. 153 – Can you expand on why the Metropolis criterion ensures
variability in the population? While this might be intuitive for experts, it might
not be for clear to the general reader of ACP. A couple of follow-up questions
on the Metropolis algorithm: Did the MCGA algorithm perform significantly better
with this criterion? Do you make sure that a newly created parameter set with
improved fitness over all previous ones is not discarded?

Response

The idea behind the Metropolis criterion (together with the mutation scheme) is that sometimes
candidates with worse goodness-of-fit are accepted to the next generation. The idea is to keep the
population more variable by removing members from the previous generation that would otherwise
be included in the next generation and thereby to allow the MCGA algorithm to explore the
parameter space more thoroughly.

The Metropolis criterion does not significantly increase the performance of the algorithm when the
versions with and without metropolis criterion are tested to artificial data set 1. Figure 2 below
shows the distribution of the median mean squared error for generations 2-10 over the 500
optimization rounds performed with the Metropolis criterion (blue lines) and MSE over 50
optimization rounds performed without the Metropolis criterion (red lines). Figure 1 shows that at
first the blue distribution is wider but not by much and in the end (generation 10) the version
without the Metropolis criterion has more probability mass over smaller and higher median MSE
values.

The Metropolis criterion is applied only for candidates that have higher MSE than the maximum
MSE in the previous generation, which ensures that a newly created parameter sets with improved
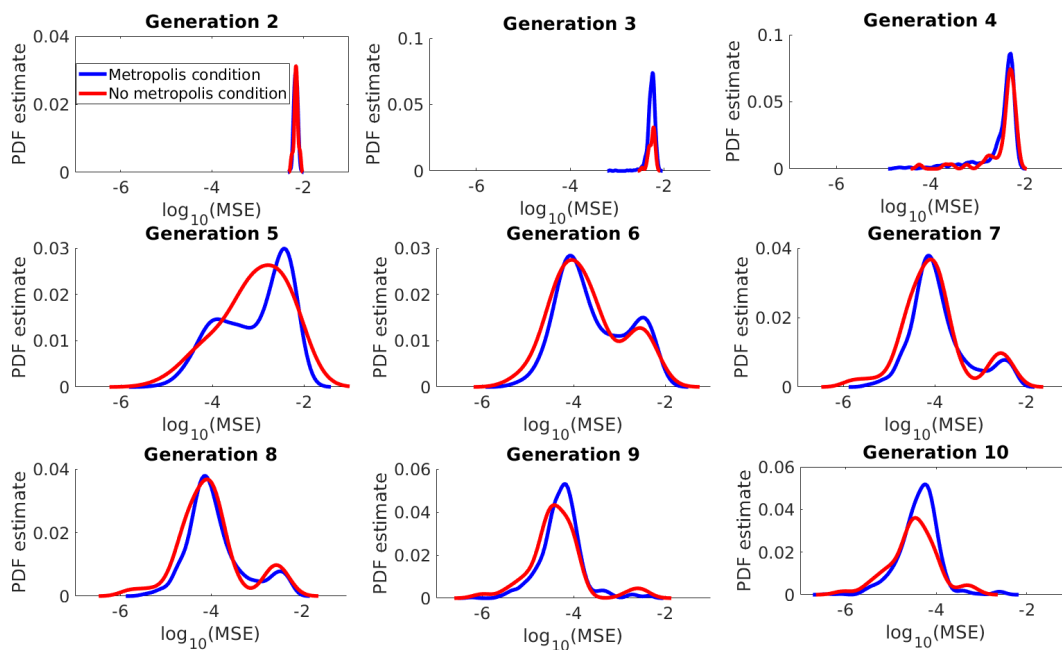fitness are not discarded.

Figure 2: Distribution of median mean squared error (MSE) in a generation for 500 optimization
rounds with the Metropolis condition and 50 optimization rounds without the Metorpolis for
artificial data set 1 in the manuscript. The distribution is calculated with a kernel density estimation
method using Gaussian kernel.

We have added a following explanation to the manuscript Sect 2.2 line 157:

In genetic algorithms the goal is to keep the population as variable as possible while at the same time the goal is that the fitness of the candidates improves when new generations are calculated. If only the candidates that best produce the observations were chosen the algorithm might get stuck in a local minimum and, on the other hand, if new random parameters are drawn too often the genetic algorithm does not converge.

Specific comment 5

Sect. 2.3.1, l. 201 – The comment on subconscious bias made me wonder what choices the person performing the optimization has. In my understanding, there should be none in a fully automated optimization.

Response

Even though the optimization is fully automated there exists a couple of things that the person performing the optimization can do to guide the optimization towards correct results, even though their effect might not be substantial to the optimization. The person performing the optimization can narrow the parameter space so that it is more likely for the algorithm to find correct values. The person might tune lower the mutation rate or increase the number of elite members in a generation if the algorithm is found to converge fast towards the correct values. One could also try different goodness-of-fit functions so that the correct values were found more likely. When analyzing real SOA evaporation experiments the correct volatility distribution is not known, therefore, the above mentioned factors cannot be used to guide the results towards correct values. In practice, the above mentioned factors include decision making by the operator but the operator has to be able to make these decisions based on technical aspects of the method and the optimization problem at hand and not by knowing the correct answers.

Specific comment 6

Sect. 4, l. 294 – Please define the term "optimization rounds". From context, it seems to be completed MCGA runs. In contrast, how many process model evaluations were performed in each MCGA run? How has this number been chosen?

Response

We have defined the optimization rounds to mean MCGA runs in Sect 2.2.1 line 161.

The number of process model evaluations was not chosen when performing the optimization, instead we chose the number of generations and population size such that further increase in either number did not decrease the mean squared error between model output and data significantly, while at the same time the choice kept the computation time as small as possible.

The number of process model evaluations can be calculated from these two numbers considering that we choose the number of parameters to sample in the MC phase to be the same as in the GA phase and that the process model evaluations in the GA part is $0.95 N_{population} \cdot (N_{generation-} 1)$, where

$N_{population}$ is the population size and $N_{generation}$ the number of generations. The coefficient 0.95 comes from the fact that 5% of the next generation is always populated with the elite members of the previous generation. This results in 6840 process model evaluations with $N_{population}= 400$ (corresponding to mixtures 3 and 4 at low RH in our study) or to .10260 evaluations with $N_{population}= 600$ (corresponding to all other data sets in our study).

We have added Table S1 to the supplement which shows the population size, number of elite members and the number of parameter sets in the MC part for each data set. This table is referred to in the manuscript in Sect 2.2.1 lines 167-168. The old table S1 showing the composition of the particle at the start of the evaporation for artificial data set 4 is now labelled as Table S2 in the revised version of the manuscript

All the MCGA parameters for each data set in this work are listed in the supplementary material Table S1.

Specific comment 7

Sect. 5.3 – You give two potential reasons for the process model failing at describing the experimental data using only literature values for viscosity and volatility. Can you add a brief discussion on what you think contributes more to the observed discrepancy, the depressed viscosity or hindered evaporation due to Raoult's law?

Response

In Sect 5.3. we speculate with the possibility that since the AIOMFAC model gives lower than unity activity coefficients for the initial particle composition, there might be more water in the particle, which would hinder the rate of evaporation of other compounds and lower viscosity. It is noteworthy that these changes would affect the rate of evaporation opposite ways. The decreased viscosity would increase the rate of evaporation, whereas solution effect would decrease the rate of evaporation of an organic compound.

We have performed the AIOMFAC calculations only with one composition (the initial particle composition) and only to consider with the possibility of more water being present at low RH measurements of mixtures 3 and 4 and at high RH measurement of mixture 3. Discussion about the magnitudes of these effects would need detailed calculations of the activity coefficients as a function of composition which is out of the scope of this study.

Specific comment 8

Sect. 6, l. 600 – "(. . .) the few shortcomings of the method could be largely attributed to the fact that the method can only characterize properties that influence the quantity that is measured". As stated, this is too trivial, please rephrase. You may want to refer to it as "model parameters that have sufficient sensitivity in the probed time and concentration range". For reference, some general concepts of model parameter optimization (at least for application in aerosol research) have been discussed in section 3 in Berkemeier et al. (2017) or can be found in the discussion of sensitivity analysis and kinetic regimes in Berkemeier et al. (2013), section 6.

Response

We have modified the text starting at line 622 in the revised version of the manuscript to read:

For some of the tested data sets, the few shortcomings of the method could be largely attributed to the fact that the model output was not sensitive to the changes in the estimated parameters with respect to the experimental timescale and parameter range.

Specific comment 9

Fig. S9 – Please add literature values from Table 5 into the plot since you are referring to this comparison in Sect. 5.3.

Response

We have added the literature values to Fig. S9.

References

Berkemeier, T., S. Steimer, S., K. Krieger, U., Peter, T., Pöschl, U., Ammann, M. and Shiraiwa, M.: Ozone uptake on glassy, semi-solid and liquid organic matter and the role of reactive oxygen intermediates in atmospheric aerosol chemistry, Phys. Chem. Chem. Phys., 18(18), 12662–12674, doi:10.1039/C6CP00634E, 2016.

Buchholz, A., Lambe, A. T., Ylisirniö, A., Li, Z., Tikkanen, O.-P., Faiola, C., Kari, E., Hao, L., Luoma, O., Huang, W., Mohr, C., Worsnop, D. R., Nizkorodov, S. A., Yli-Juuti, T., Schobesberger, S. and Virtanen, A.: Insights into the O;C-dependent mechanisms controlling the evaporation of α-pinene secondary organic aerosol particles, Atmospheric Chem. Phys., 19(6), 4061–4073, doi:10.5194/acp-19-4061-2019, 2019.

Lowe, S., Partridge, D. G., Topping, D. and Stier, P.: Inverse modelling of Köhler theory – Part 1: A response surface analysis of CCN spectra with respect to surface-active organic species, Atmospheric Chem. Phys., 16(17), 10941–10963, doi:https://doi.org/10.5194/acp-16-10941-2016, 2016.

Yli-Juuti, T., Pajunoja, A., Tikkanen, O.-P., Buchholz, A., Faiola, C., Väisänen, O., Hao, L., Kari, E., Peräkylä, O., Garmash, O., Shiraiwa, M., Ehn, M., Lehtinen, K. and Virtanen, A.: Factors controlling the evaporation of secondary organic aerosol from α-pinene ozonolysis, Geophys. Res. Lett., 44(5), 2016GL072364, doi:10.1002/2016GL072364, 2017.

Optimization of process models for determining volatility distribution and viscosity of organic aerosols from isothermal particle evaporation data

Olli-Pekka Tikkanen[1], Väinö Hämäläinen[1], Grazia Rovelli[2], Antti Lipponen[3], Manabu Shiraiwa[4], Jonathan P. Reid[2], Kari E. J. Lehtinen[1,3] and Taina Yli-Juuti[1]

[1]Department of Applied Physics, University of Eastern Finland, Kuopio, Finland
[2]School of Chemistry, University of Bristol, Bristol, BS8 1TS, UK
[3]Atmospheric Research Centre of Eastern Finland, Finnish Meteorological Institute, Kuopio, Finland
[4]Department of Chemistry, University of California, Irvine, CA, USA

Correspondence to: Olli-Pekka Tikkanen (op.tikkanen@uef.fi)

Abstract.

The composition of organic aerosol under different ambient conditions as well as their phase state have been a subject of intense study in the recent years. One way to study the particle properties is to measure the particle size shrinkage in a diluted environment at isothermal conditions. From these measurements it is possible to separate the fraction of low volatility compounds from high volatility compounds. In this work, we analyze and evaluate a method for obtaining particle composition and viscosity from measurements using process models coupled with input optimization algorithms. Two optimization methods, Monte Carlo Genetic Algorithm and Bayesian inference, are used together with process models describing the dynamics of particle evaporation. The process model optimization scheme in inferring particle composition in a volatility-basis-set sense and composition dependent particle viscosity is tested with artificially generated data sets and real experimental data. Optimizing model input so that the output matches these data yields a good match for the estimated quantities. Both optimization methods give equally good results when they are used to estimate particle composition to artificial test data. The time scale of the experiments and the initial particle size are found to be important in defining the range of values that can be identified for the properties from the optimization.

1 Introduction

It has been estimated that organic aerosols (OA) comprise a large fraction of global aerosol particle mass (Kanakidou et al., 2005; Jimenez et al., 2009) A significant fraction of OA is of secondary origin (Secondary Organic Aerosol, SOA) i.e. OA formed from oxidation of volatile organic compounds and their subsequent condensation onto pre-existing particles (Hallquist et al., 2009). Especially in SOA systems, there are gaps of knowledge in the composition and phase state of the particles and their response to atmospheric conditions such as relative humidity or temperature (Hallquist et al., 2009;

1

Virtanen et al., 2010; Pajunoja et al., 2015). These properties are important since they control the evolution of atmospheric organic particles and their subsequent effect to climate (Tsigaridis et al., 2014; Shiraiwa et al., 2017).

35

The volatilities of particle phase compounds in OA and the viscosity of the particles can be inferred by measuring the size change of particles during their evaporation (Vaden et al., 2011; Wilson et al., 2015; Yli-Juuti et al., 2017). In addition, if the shrinking stops after a certain time, the particles can be inferred to contain organic compounds which are non-volatile with respect to the ambient conditions. The phase state of OA particles can be studied in these experiments by comparing

40   evaporation at different relative humidity conditions. New techniques have also been developed to infer the viscosity of the particles directly (Abramson et al., 2013; Renbaum-Wolff et al., 2013; Reid et al., 2018). The benefit of the evaporation technique over direct measurement of viscosity is the possibility of using freshly formed, suspended OA particles without a need, for example, for filter collection and further treatment.

45   In addition to experimental methods, increasing attention has also been given to modeling the evaporation process ~~particle dynamics~~ to better understand the measurements (Vaden et al., 2011; Liu et al., 2016; Yli-Juuti et al., 2017). Usually, the model results obtained by assuming distinct OA properties are compared to experimental data and conclusions are drawn from the differences or similarities of the two. However, an inverse approach is also possible where some of the OA properties are fit such that the model output is matched to the experimental observations. This approach allows the

50   estimation of the properties that are challenging to measure directly with available instruments. For example, Arangio et al. (2015) used this concept to derive kinetic parameters for multiphase chemical reactions of hydroxyl radical with levoglucosan and abietic acid. Berkemeier et al., (2016)~~Berkemeier et al., (2016)~~ derived kinetic parameters influencing ozone uptake of shikimic acid by fitting to multiple measurements of ozone uptake by the acid at different relative humidities. Lowe et al., (2016) studied the sensitivity of various parameters of Köhler theory by studying the goodness-of-fit

55   to artificial cloud condensation nucleus spectra. ~~The same approach was also used by~~ Yli-Juuti et al. (2017) ~~to~~ inferred volatility distribution of compounds in SOA particles by searching for an optimal input to a process model such that the model produces similar particle size change as was measured.

Even though the optimization of models to replicate experimental data is a widely used method in other fields (e.g., Kaipio et

60   al., 2000; Hernández et al., 2017; Varvia et al., 2018), such an approach is yet to be commonly utilized in studies probing organic aerosol volatility and viscosity. The current challenges of estimating accurately OA component volatility and particle viscosity raises a need for studies that assess how accurately they can be inferred by fitting process model output to time dependent evaporation measurements, which is the aim of this study.

65   The rest of the article is organized as follows. In the second section the evaporation data and computational methods are described. In the third section two different approaches for performing the optimization are tested. In sections four and five,

2

the particle volatility distribution is optimized to match artificial data sets and then the optimization method is tested by applying it to experimental data sets where the composition and viscosity of generated particles are known. In the last section the findings are summarized and conclusions are drawn.

2 Methods

The optimization method described here is based on process models that simulate the evaporation of OA particles and an optimization algorithm that is used for finding the desired properties. Two evaporation models which have different levels of detail in their representation of the aerosol particle evaporation process are used. Additionally, two different optimization algorithms are tested.

2.1 Process models

Evaporation at high relative humidity (RH) is modelled with a liquid-like evaporation model (hereafter LLEVAP) (Yli-Juuti et al., 2017) and evaporation at low RH with a modified version of the kinetic multi-layer model for gas-particle interactions in aerosols and clouds (KM-GAP) model (Shiraiwa et al., 2012; Yli-Juuti et al., 2017). Both models and variations from their typical implementations are described below.

In LLEVAP the evaporation of an organic compound i is controlled by the difference in its gas phase concentration C_i and the equilibrium concentration $C_{eq,i}$ (Vesala et al., 1997; Lehtinen and Kulmala, 2003), equivalent to the gas phase diffusional gradient between the infinite distance and particle surface, respectively. Therefore, the mass transport between the gas and the particle phase is assumed to be the limiting phenomenon and the diffusion timescales within the particle are assumed to be negligible. The mixture of organics and water is assumed to behave ideally. When performing optimization to interpret real measurements, as described in Sect. 2.3.2, a flow of N_2 maintains a near-zero background gas phase concentration of the volatilizing components. This nitrogen flow is taken into account by including the Sherwood number correction to the mass flux equations (Kulmala et al., 1995).

In KM-GAP, the particle phase mass transport is modelled by dividing the particle into concentric layers (Shiraiwa et al., 2012, 2013). The composition dependent viscosity η in layer j is assumed to have a form

$$\log_{10}(\eta_j) = \sum_{i=1}^{N} X_{mole,i,j} \log_{10}(b_i),$$

(1)

where $X_{mole,i,j}$ is the mole fraction of the ith compound in jth layer and b_i is a coefficient that describes the contribution of compound I to the viscosity η_j (O'Meara et al., 2016). The particle phase diffusion coefficients are calculated from the viscosities based on the Stokes-Einstein relation (Einstein, 1905). The molecular diffusion inside the particle is calculated based on the Fick's law of diffusion. As with LLEVAP, an ideal mixture is assumed in the KM-GAP model implementation.

3

During an evaporation simulation the particle size decreases. This shrinkage is modelled by allowing the quasi-static surface layer (the outermost layer of the particle) to shrink so that its thickness deviates from the thicknesses of other layers. If the thickness of the quasi-static surface layer is less than 0.3 nm it is combined with the first bulk layer which is the layer directly beneath the quasi-static surface layer. This approach is the same that was used by Yli-Juuti et al. (2017).

In both models, equilibrium partitioning of water in gas and particle phases is assumed. In LLEVAP, this controls the mole fraction of water in the entire particle. In KM-GAP, this assumption controls the mole fraction of water in the particle surface layer while the composition of the inner layers is based on the kinetics of water transport. Moreover, the coefficient b for water in equation (1) is set to the literature value for the viscosity of pure water, $b_{water} \approx 10^{-3}$ Pa s (Rumble et al., 2018) when calculating the viscosity of a mixture in a layer.

In most of the model simulations the organic compounds are represented by a one dimensional volatility basis set (Donahue et al., 2006) (1D-VBS, hereafter VBS). Organic compounds are grouped into distinct 'bins' in a VBS, described by their saturation (mass) concentration (C_{sat}) value and the amount of that bin in gas and particle phases. The saturation concentration of a compound can be used interchangeably with the effective saturation concentration ($C_{sat,i}$ times the activity coefficient of compound i) C^{*}_{i} because the organic-water mixture is assumed to behave ideally.

The volatilities of the compounds in the particle are modelled with either a "full VBS" or with a "sparse VBS". The full VBS consists of bins from minimum defined C_{sat} to maximum defined C_{sat} with a decadal difference in C_{sat} between two adjacent bins; the sparse VBS consists of a predefined number of bins whose saturation concentration is not constrained relative to each other. The sparse VBS is used to present the properties of the organic compounds where the number of evaporating compounds is known. From hereafter the terms compound and VBS bin are used interchangeably in the text. The gas phase is assumed to be infinitely diluted of organic compounds in the particle evaporation data sets described in Sect. 2.3 and, thus, the mass or mole fraction presented in the VBS is always the fraction in the particle phase.

2.2 Optimization methods

2.2.1 Monte Carlo Genetic Algorithm

The Monte Carlo Genetic Algorithm (MCGA) is an optimization method developed by Berkemeier et al., 2017~~Berkemeier et al., 2017~~. MCGA has been previously used in estimating atmospheric multiphase chemistry parameters such as reaction rate coefficients and bulk phase diffusion coefficients (Table 1 in Berkemeier et al., 2017)~~(Table 1 in Berkemeier et al., 2017)~~.

The algorithm divides the optimization process into two different parts: a random sampling of the parameter space (MC part) and a genetic algorithm (GA part) with an initial population from the MC sampling. Random sampling means that a predetermined number of parameter sets, named candidate solutions or candidates, are created by randomly choosing values for the free parameters (Berkemeier et al., 2017)~~(Berkemeier et al., 2017)~~. These candidates form a population. The free parameter values are drawn from a uniform distribution between 0.01 and 1 for the mole or mass fraction of a compound and from a log-uniform distribution for the saturation concentrations and b-parameters of equation (1), with clearly defined minimum and maximum values (see Table 1 and Table 4~~3~~). Below t~~T~~he fitness ~~goodness~~ of a candidate is determined ~~by calculating~~as the inverse of its goodness of fit statistic~~fitness~~. The goodness of fit ~~fitness~~ in this work is calculated as a mean squared error (MSE) between the evaporation simulation produced with the candidate's parameter set and the measured evaporation. A lower value for goodness of fit statistic, i.e. lower MSE, means ~~lower~~higher value for fitness ~~means~~and a better candidate.

The initial population to the GA part is chosen from the MC part so that 5% of the best-fit candidates are chosen and the remaining 95% of the population is chosen randomly. The computation times of the MC and GA parts are divided, so that both parts require about half of the total computation time (Berkemeier et al., 2017)~~(Berkemeier et al., 2017)~~.

The GA part employs a survival-of-the-fittest scheme to improve the parameter sets drawn in the MC part. The GA part consists of evolving the initial population by forming generations. Each new generation is created by first choosing a number of elite candidates from the previous generation whose fitness ~~value~~ is the highest~~lowest~~. The rest of the generation is created in a crossover process. First two candidates, called parents, are chosen. A new candidate is created from the two parents' parameter sets. A new parameter for the new candidate is chosen from the parents' parameters randomly (Berkemeier et al., 2017)~~(Berkemeier et al., 2017)~~.

The version of the algorithm used in this work differs from the version described in Berkemeier et al., (2017)~~Berkemeier et al., (2017)~~ in that how a new candidate is accepted to the next generation and how parents are chosen. Once the new candidate has all its free parameters drawn, it is accepted to the new generation if its fitness is higher ~~lower~~ than the lowest~~largest~~ fitness in the previous generation or if candidate's fitness divided by the lowest fitness in the previous generation is lower ~~lower fitness in the previous generation divided by the candidate's fitness is largest~~the~~ than a uniform random number between 0 and 1. If neither of the criteria for accepting the candidate is met, a parent survives to the next generation with probability proportional to their MSE ~~fitness~~ values. The additional criterion for accepting the candidate is similar to the Metropolis algorithm (Metropolis et al., 1953). Lastly in the GA, once a new candidate is created and before its fitness is compared against the previous generation, the candidate can undergo mutation with a preset probability. If mutation happens the values for all the fitting parameters are chosen again randomly. In genetic algorithms the goal is to keep the population as variable as possible while at the same time improving the fitness of the candidates when new generations are calculated. If

only the candidates that best produce the observations were chosen, the algorithm might get stuck in a local minimum and, on the other hand, if new random parameters were drawn too often the genetic algorithm would not converge. The mutation step together with the Metropolis criterion ensures that the values of the fitting parameters stay variable in the population.

The probability to be chosen to be a parent was set to be ~~inversely~~ proportional to the candidate's fitness. This way the parameters that produce better fits to the data are more likely chosen than those candidates that produce worse fits. The number of elite candidates was set to be 5% of the generation size and the mutation probability was set to 20%. The number of generations was set to 10. To get statistics of the estimated parameters the optimization process was always repeated at least 100 times. These consecutive optimization runs are hereafter referred as optimization rounds. All the MCGA parameters for each data sets in this work are listed in the supplementary material Table S1.

When showing estimates from the distribution of fitted parameters, the mode of the estimate is used as a point estimate and the uncertainty is characterized by the 10th and 90th percentiles of the distribution.

2.2.2. Bayesian inference

Bayesian inference is a class of statistical inference that can be used in finding estimates for unknown parameters in a model. In Bayesian inference, the estimates of the unknown parameters are based on statistical prior information, observed data and an observation model. Statistical prior information is encoded into prior probability distribution and it can be used, for example, to constrain the unknown parameter values to a physically feasible range (e.g. non-negativity). The observation model describes the dependency between the observed data and unknown parameters, and statistical models for the observation noise and model uncertainties are used to construct the so-called likelihood probability distribution. The solution of a Bayesian inference problem is a posterior probability distribution that is a conditional probability distribution for the unknown parameters given the observations and prior information. The posterior probability according to the Bayes' rule (Bayes et al., 1763; Gelman et al., 2013) is proportional to the product of likelihood and prior probabilities. Usually in practical applications, the posterior probability distribution is not used as it is, but it is used to derive point or interval estimates for the unknown parameters.

Analytic derivation of the posterior probability distribution is often difficult or even impossible and, therefore, feasible numerical methods have been developed to explore the posterior probability distribution. These numerical methods are typically used to draw random samples from the posterior probability distribution. The random samples are further used to compute point estimates and credible intervals for the unknown parameters. A well-known class of sampling algorithms are the Markov Chain Monte Carlo (MCMC) algorithms. In MCMC algorithms, random samples from the posterior probability distributions are drawn and, for example, the most probable values for the unknown parameters are computed.

The evaporation of an organic aerosol particle is modelled using the LLEVAP model described in Sect. 2.1. This method is applied to data set 1 described in Sect. 2.3. The prior probability models for the three organic compounds in data set 1 are set to positive parts of normal distributions with means of 0, 0 and 500 μg m^{-3} and standard deviations of 10, 10 and 500 μg m^{-3}, respectively for the saturation concentrations of the three organic compounds. For the molar fraction the mean is 1/3, standard deviation is 1/3 and the distributions Gaussian for every compound with the negative part of the distribution function removed. A Hamiltonian MCMC algorithm the No-U-Turn Sampler (NUTS) (Hoffman and Gelman, 2014) is employed using the Stan software (Carpenter et al., 2017) to draw 2000 samples from the posterior probability distribution. Finally, the most probable random sample according to the posterior distribution are taken as the point estimate for the unknown parameters. This point estimate is called the maximum a posteriori (MAP) estimate. Furthermore, the 90% credible interval for the unknown parameters is calculated to reflect the uncertainty of the estimates.

2.3. Test data

Altogether, ten different data sets were used to test how well the volatility and viscosity of OA particles can be estimated using the techniques described above. First, four artificially created data sets were used to test the accuracy of the estimated VBS in case of no particle phase diffusion limitations. Second, particle evaporation data measured with an Electrodynamic Balance (EDB) (see Sect. 2.3.2) were used to characterize how well the volatility of compounds can be estimated from experimental data on particles consisting of few compounds. Finally, measured evaporation data were used to test the simultaneous estimation of volatility and viscosity of particles generated from two compound mixtures.

2.3.1 Artificial data sets generated with LLEVAP model

All the four artificial data sets were generated using the LLEVAP model. In every case the data sets were created by a different person than the one performing the optimization. This prevented subconscious bias, with the operator altering the estimates towards correct values. Table 1 shows the properties of the particles or the organic compounds that change between data sets and the free parameters. Table 2 shows the properties of the organic compounds and ambient conditions that are the same between the data sets and Table 3 shows the mole fractions and saturation concentrations of each compound in every data set. The optimization results of these data sets are described and discussed in Sect. 4. Additionally, the first artificial data set is also used to compare the Bayesian inference and MCGA methods in Sect. 3.

The artificial data sets 1,3 and 4 mimic evaporation of monodisperse particle population in the University of Eastern Finland residence time chamber similar to the measurements reported in Yli-Juuti et al., (2017). The data sets differ in their number of organic compounds and their saturation concentration values. In data set 1, three organic compounds were used and their C_{sat} values were chosen from the appropriate range. Both saturation concentrations and initial dry mole fractions of the compounds in the particle were treated as free parameters in optimization. In data set 3, six organic compounds, i.e. a full

VBS, were used. The saturation concentrations were set to their correct values (see Table 1) and only dry particle mole fractions at the start of the evaporation were optimized. Data set 4 was generated by simulating evaporation of a mixture of 40 compounds with a range of C_{sat} and mole fractions. In optimization a full VBS with fixed saturation concentrations was used.

Artificial data set 2 mimics the evaporation of a single particle in an Electrodynamic Balance (see next subsection). This data set simulates the particle evaporation measurements performed at the University of Bristol (Davies et al., 2012; Rovelli et al., 2016). Data set 2 differs from the other data sets as the particle diameter is larger by several orders of magnitude at the start of the evaporation and the particle size is sampled at a higher frequency. The number of organic compounds in data set 2 was set to three and both the values of saturation concentration and the initial fraction of each organic compound was optimized to fit the data (similar to data set 1). The artificial evaporation data are shown in Fig. 1 as well as in the supplement (Fig. S1, Fig. S2, Fig. S3 and Fig. S4).

2.3.2 Experimental OA evaporation data

An Electrodynamic Balance (EDB) was used to trap single aerosol droplets generated from aqueous mixtures of organic components with known chemical composition. The evaporative loss of semi-volatile organic components was observed by measuring changes in the droplet radius over timescales of $\sim 10^5$ s. The experimental setup and the sizing of trapped droplets is extensively described in previous publications (Davies et al., 2013; Rovelli et al., 2016; Marsh et al., 2017) and briefly presented below.

Charged droplets are generated by means of a microdispenser (Microfab MJ-ABP-01) and confined within the electrodynamic field generated by a set of concentric cylindrical electrodes. Once trapped, a single particle sits in a nitrogen flow (200 mL min^{-1}, gas flow velocity of 3 cm s^{-1}) of controlled RH and T. The RH is measured by fitting either the size vs. time profile of an evaporating probe water droplet (at RHs above 80%) or the equilibrated radius of a NaCl or NaNO$_3$ aqueous solution probe droplet (below 80%) by applying a literature evaporation/condensation kinetic model (Kulmala et al., 1993). The procedure is described in Rovelli et al. (2016), where the uncertainties associated with the measured RH are also discussed (typically <±0.2% at RH > 90% and ~±1% below 90%). The temperature is measured by means of a thermocouple (NI-USB-TC01, thermocouple type K, uncertainty of ±1.5 K) placed between the inner and the outer bottom electrodes, directly within the gas flow. All the measurements in this work have been taken at 293 K. The droplet is illuminated with a 532 nm laser light (Laser Quantum Ventus CW laser) and the angularly-resolved elastically scattered light is collected with a camera (Thorlabs CMOS camera, DCC1545M). The scattering pattern is used to retrieve the evolving radius of the confined droplet, by applying the geometric optics approximation (Glantschnig and Chen, 1981), with a time resolution up to 10 ms.

Four different aqueous mixtures of organic components were considered; their detailed chemical composition can be found in Table 4̶3. Mixtures 1 and 2 include three components of variable volatility, whereas Mixtures 3 and 4 are sucrose-glycerol-water ternary solutions. Considering that the water activity-dependent viscosity of binary sucrose spans over 10^{-3}-10^{12}

260   Pa s (Power et al., 2013) and that pure glycerol has a viscosity of 1.46 Pa s (Haynes, 2009), the viscosity of Mixture 3 and 4 is expected to be significant and to increase over time as glycerol evaporates from the trapped droplet. For each of these mixtures, a single droplet was trapped into two different RHs (low and high RH, see sect. 5.2).

3 Comparison of MCGA and Bayesian inference methods for fitting volatility

The artificial data set 1 was used to compare the two estimation methods, MCGA and Bayesian inference. Estimates for

265   three saturation concentrations and dry particle mole fractions at the start of the evaporation were calculated. For MCGA, the total number of optimization rounds was 500. For Bayesian inference, 2000 samples were generated after a burn-in period of 500 samples where the parameters of the NUTS algorithm were tuned (Hoffman and Gelman, 2014). Every fourth estimated parameter set was selected from these 2000 samples for the final analysis allowing the two methods to be compared.

270   Additionally, the MCGA method was used with two different sampling schemes. In the uniform sampling scheme, the fitting parameter values were drawn from a uniform distribution (log-uniform distribution for C_{sat}). In the second scheme the values for saturation concentration and mole fractions at the start of the evaporation are drawn from a normal distribution with preset means and standard deviations similar to the Bayesian inference method (see Sect. 2.2.2). The two MCGA schemes are later referenced as MCGA with uniform sampling and Gaussian sampling, respectively.

275

Bayesian inference fundamentally assumes that experimental values are always associated with an uncertainty. This uncertainty is needed as an *a priori* knowledge before any Bayesian analysis can take place. The artificial data set 1, however, did not include any uncertainty. When optimizing the particle composition with the Bayesian inference method, a 1% uncertainty in the evaporation factor (EF) (particle diameter divided by the initial diameter) was assumed.

280

The Bayesian inference and the MCMC algorithm assume estimated parameters are random variables with probability distributions, whereas the MCGA algorithm tries to find a single set of input parameters that best fit to the observations. The MCMC algorithm explores the posterior distribution by randomly drawing samples from it. The samples are drawn such that the parameter values that better fit to the data and thus are more probable are drawn more often than the lower probability

285   parameter values that produce worse fits. Because of this fundamental difference between these two approaches, it would not be appropriate to compare how the model output-data residuals evolve during the execution of both algorithms and only the

9

290   Overall the three methods are able to produce similar, reliable estimates that are close to the correct values (Fig. 2). Figure S1 shows the relative evaporation curve densities for all the three optimization methods together with the artificial evaporation data. Relative curve density is calculated by dividing the time and EF space into grids and calculating how many of the simulated evaporation curves go through a specific grid point and dividing this count by the maximum count in the same time column. The relative curve densities are similar for the three methods (Fig. S1).

295

The differences between the methods are the most obvious with the most volatile compound. While the mole fraction estimates are all close to the correct value, the saturation concentration estimates show deviation from the correct value. The Bayesian inference estimate (1230 μg m^{-3}) narrowly misses the correct saturation concentration (1000 μg m^{-3}). The MCGA method with Gaussian sampling produces an estimate of 800 μg m^{-3}, a difference opposite in direction to the Bayesian

300   inference method. The estimate with the MCGA method with uniform sampling deviates the most from the correct value (600 μg m^{-3}). The absolute uncertainties of all the three methods span over several hundred of μg m^{-3}. The reason for this high uncertainty is due to the evaporation time scale of the highest volatility compound and is discussed more thoroughly in Sect. 4.1.

305   Since all of the studied optimization methods yielded similar results, only the MCGA scheme with uniform sampling is used in the rest of this study, first to test the optimization method with different artificial data sets and then with the experimental data.

4 Evaluation of process model optimization method for fitting OA properties to artificial test data

The estimates of the compounds with highest and lowest volatility in data set 1 are more uncertain than the estimates of the

310   other compounds. In this section the reasons for this behavior are examined. Further, the process model optimization scheme is tested in estimating volatility for the three remaining artificial data sets. With data set 2, the goal is to inspect the performance of the process model input optimization approach when the evaporation conditions change in terms of particle diameter, evaporation timescale and measurement sampling frequency. With data set 3, the target is to evaluate the performance of the optimization in the case of a full VBS and the method's ability to distinguish VBS bins from each other.

315   With data set 4 the optimization method is tested against evaporation data where the particle contains more evaporating compounds than what are used in the optimization which is the case with real OA. 500 optimization rounds were calculated for every data set.

10

The range of saturation concentrations that can be determined from the data with the optimization method varies with initial
320 particle diameter and with the timespan of the evaporation data. The former is due to the dependence of the mass flux between the gas and particle phases on particle size. To assess the range of minimum and maximum possible saturation concentrations that can be identified with the method from data sets, the LLEVAP model was run multiple times with particles that consist solely of one evaporating component and are characterized by variable size. The minimum identifiable saturation concentration was determined to be the concentration that shows at least 1% shrinkage in terms of particle
325 diameter in the time scale of an experiment. Similarly, the maximum identifiable saturation concentration was determined to correspond to a concentration that left 10% of the particle size remaining at first data point. These minimum and maximum values are shown in Table 1. The evaporation rate of a compound depends also on its mole fraction, but this simple analysis already gives reasonable range of possible saturation concentrations for the optimization process.

4.1 Data set 1

330 The values of estimated variables in Fig. 2 show the largest uncertainty for the lowest and highest volatility compound whereas the middle saturation concentration compound has a relatively small uncertainty. The reason for this behavior lies in the nature of the evaporation process. For the least volatile compound, the correct value of the estimated saturation concentration was 0.01 μg m^{-3}. The 10th and 90th percentiles of the obtained estimate were 0.004 μg m^{-3} and 0.012 μg m^{-3}. The lower end of the estimated saturation concentrations corresponds to evaporation curves which do not practically show any
335 evaporation once the middle volatility compound has evaporated from the particles. The higher end corresponds to curves which follow the slow evaporation pattern also observed in the data. To constrain the saturation concentration and mole fraction estimates of the least volatile compound better, more data would be needed after ca. 50 minutes, when the evaporation of the least volatile compound dominates the particle shrinkage.

340 A similar analysis can be applied to the most volatile compound, for which the obtained values of saturation concentration span from around 400 μg m^{-3} to over 3000 μg m^{-3}. In the case of data set 1, the amount of the most volatile compound decreases by 99% during the first 5 seconds of the evaporation. As there is only one data point before 5 s, the estimated values of the most volatile compound contribute relatively little compared to the other two compounds when the goodness of fit is calculated. In all simulations there exists a distinct high volatility compound as the shape of the evaporation curve
345 dictates that the particle must shrink 10% by diameter during the first 10 minutes. This shrinkage can only be achieved with a compound that has a relatively high saturation concentration. More accurate estimates of the most volatile compound would require more data points at the very beginning of the evaporation. As data set 1 mimics evaporation experiments which require filling of an evaporation chamber as reported in Yli-Juuti et al. (2017), it might not be straightforward to obtain more data points at the start of the evaporation.

350

4.2 Data set 2

There exist three key differences in data set 2 compared to other data sets. First, the data extends almost twice as long in time. Second, the particle diameter is 125 times larger and, third, the time resolution is higher resulting in more data points especially at the start of the evaporation. The first two differences mean that the range of identifiable C_{sat} values changes compared to data sets 1,3 and 4 (see Table 1).

The MCGA estimates agree well with the correct values for data set 2 (Fig. 3). For the least volatile compound the saturation concentration and mole fraction estimates match exactly with the correct values. The uncertainty in the mole fraction estimate is small. While at first the uncertainty in the saturation concentration might seem high for the least volatile component, the absolute values are between 0.4 μg m^{-3} and 20 μg m^{-3} and organics with these saturation concentrations do not evaporate at all or evaporate only very slowly in the timescale of the simulated evaporation.

The estimates for the second compound match the correct values well. The behavior is similar to data set 1, for which it was found that the compound whose saturation concentration lies between the two other compounds' saturation concentration was characterized the best.

For the most volatile compounds the estimates are close to the correct values and the uncertainty in mole fraction is negligible. The uncertainty in the C_{sat} estimate is high and rises from the fact that only ca. 8% of the data points are recorded before the most volatile compound is gone (over the timescale of ca. 30 s). However, the increased number in data points that influence C_{sat} value makes the estimate more certain when compared to the estimate of the most volatile compound calculated with MCGA and uniform sampling of the parameters in data set 1 for which only one data point is encountered before the compound has practically evaporated.

4.3 Data set 3

Artificial data set 3 describes the evaporation of organic aerosol in similar conditions as data set 1. The difference from data set 1 is that the particle composition consists of a "full VBS" i.e. all VBS bins between minimum and maximum identifiable C_{sat} are present in the particle at the start of the evaporation. From the optimization point-of-view, the saturation concentrations of the organic compounds are fixed during the optimization and only the mole fractions of each compound at the start of the evaporation are optimized to the data. This mimics the analysis that would be performed for SOA particles to derive their composition in terms of a full volatility distribution. The estimated mole fractions together with the correct values are shown in Fig. 4. The estimated values show that when the saturation concentrations are discretized into 6 bins, optimizing only the mole fractions is more accurate compared to data set 1 where saturation concentrations and mole fractions were estimated.

For the three compounds with saturation concentration higher or equal to 10^{-1} µg m^{-3} in data set 3, the estimated mole fractions deviate only by 0.02 from the correct values. The estimates for the two least volatile compounds are different compared with the other compounds in terms of uncertainty. The estimated mole fraction for the compound with $C_{sat} = 10^{-2}$ µg m^{-3} matches the correct value and the uncertainty is -0.08 / +0.06. For the least volatile compound the estimated mole fraction is 0.01 lower than the correct value and the uncertainty is -0.04 / +0.08.

The evaporation curves calculated with the LLEVAP model using the MCGA estimates as input variables show that all the curves match artificial data set 3 extraordinarily well (Fig. 1c and Fig. S3) compared to data set 1 (Fig. 1a and Fig. S1) where the curves calculated from estimates show much higher variance around the data points. This demonstrates that the uncertainty in the mole fraction estimates is not due to the MCGA algorithm itself but to the ability to distinguish low volatility VBS bins. In fact, the same evaporation curve can be simulated by switching the amounts of molecules between the two least volatile bins. This indistinguishability is seen also in that the summed mole fraction of the two least volatile compounds is always in the range 0.35±0.01.

4.4 Data set 4

In terms of evaporation characteristics, the artificial data set 4 is similar to data sets 1 and 3. However, the evaporating particle is made of 40 different compounds for data set 4 with distinct saturation concentrations and amounts in the particle. The correct values for all the evaporating compounds can be found in Table S2‡, whereas the correct values in Fig. 5 show these forty compounds lumped into 6 VBS bins.

When optimizing the particle composition of data set 4, the compounds are presented with a full VBS similar to data set 3 and the free parameters are set the same way.

Figure 5 compares the MCGA estimates for the mole fraction with the correct values. The accuracy of the estimates is similar to the results obtained with data set 3. For the four highest volatility classes, the estimates deviate at most by 0.04 from the correct lumped values. For the two lowest volatility groups the estimates deviate more from the correct values, by approximately 0.12 for the group with $C_{sat}=10^{-2}$ µg m^{-3} and by 0.13 for the lowest volatility group. There is no consistent over- or underestimation associated to these low volatility bins. The estimate for the group with $C_{sat}=10^{-2}$ µg m^{-3} is higher than the correct value and the estimate for the lowest volatility group lower than the correct value. In both cases, the correct lumped value is included in the uncertainties of the estimates that are higher compared to the other compounds. This behavior was also seen with data set 3 and again shows the indistinguishability that is associated with the two least volatile bins and the time scale of this data set. When the sums of the two least volatile compounds are compared, the correct mole fraction would be approximately 0.58 and the 10th and 90th percentiles of the estimates are 0.58 and 0.61, respectively.

4.5 Discussion on estimating the volatility from artificial data

While all the estimates capture the correct values with reasonable accuracy, the amount of data points and their temporal distribution clearly affect the estimates. When the data are sparse, the uncertainty of the estimated variables increases as the optimization process is designed to weight each data point equally. In the case of data set 1 and data set 2, the compounds
420 with saturation concentration between the other two saturation concentrations always have the smallest uncertainty. This is because the middle compound evaporates during almost the whole duration of the data and, thus, its saturation concentration and mole fraction influences the evaporation curve the most. If the goal is to reduce uncertainties of the least volatile compound, measurements should be carried out over longer time scales. Similarly, if the goal is to study compounds that evaporate quickly, the very start of the evaporation needs to be measured at higher frequency.

425

The above results show the particle size and time scale of the experiment affect the range of possible saturation concentrations that can be estimated from the data. When the particle size is small and the measurement timescales long, lower saturation concentrations can be distinguished from the data; when the particle size is large, higher saturation concentrations are distinguished from the data. The time of the first data point and the time resolution at the start of the
430 evaporation also matter. With higher sampling frequency and earlier data points, the higher volatility compounds can be identified from the data with the optimization method.

An interesting remark concerns the choice of the variables that are optimized. From Fig. S1 and Fig. S2 it can be seen that the simulated evaporation curves show more variance around the data points when the saturation concentrations and mole
435 fractions are optimized than in Fig. S3 and Fig. S4, where only mole fractions at the start of the evaporation of a full VBS are optimized. The mole fractions are an easier task to optimize because each new VBS bin creates a new dimension to the parameter space, which can take values between zero and one. By contrast, adding a new saturation concentration dimension increases the parameter space significantly more as possible values span over several orders of magnitude.

440 It should be noted that it is not always better to fit a full VBS as illustrated by data set 3. If the number of evaporating compounds is known, fixing the number of compounds and optimizing their relative amount and saturation concentration gives more information about the experiment than optimizing only the mole fractions of a full VBS.

5 Volatility and viscosity estimates from the EDB evaporation measurements

So far, this study has considered only artificial evaporation data calculated with the LLEVAP model. Next, the process
445 model optimization scheme is applied to real experimental data. In the following discussion, "low viscosity" refers to particles where particle phase diffusivity is fast enough so that it doesn't pose a limitation to the evaporation of the volatile compounds and "high viscosity" refers to particles where the particle phase diffusivity is low enough to affect the particles'

14

evaporation rate. ~~-~~Composition are estimated for two low ~~non-~~viscosity~~us~~ (mixtures 1 and 2) and two high viscosity~~us~~ mixtures (mixtures 3 and 4 at low RH). For the latter two, the viscosities are also estimated by using evaporation profiles measured at two different relative humidities. The organic properties in the model and conditions of evaporation for all the four mixtures are listed in Table 5~~4~~. For every mixture, 100 different parameter sets that fit to the measured data were calculated. The measured and modelled evaporation curves are shown in Fig. 6 as well as in the supplement (Fig. S5, Fig S6, Fig. S7, Fig. S8)

In the EDB the particle and gas phase water are not fully in equilibrium when the measurement starts. This creates a period of very rapid evaporation when water evaporates from the particle. As both process models used in this study assume that the water is in equilibrium at the start of the evaporation, these rapid evaporation periods were removed from the data. The point at which water is in equilibrium was determined to be the point where the rate of change of particle squared radius is constantly higher than $1 \ \mu m^2 s^{-1}$ for mixtures 1,2,4 and 3 at high RH and $0.1 \ \mu m^2 s^{-1}$ for mixture 3 at low RH. The reason for the higher threshold for mixture 3 at low RH is that the mixture has the highest~~is the most~~ viscosity~~us~~ and the excess water evaporation the slowest of all the organic-water mixtures.

The sampling frequency varied across the measurements. After removing the period where water evaporates from the particle, the start of the data sets contained a period where the particle size was sampled at higher frequency than at later time. For mixture 3 at low RH and for mixture 4 at both RH this led the MCGA algorithm to weight more strongly in the fitting the start of the evaporation where there was more data. As this was not the desired behavior, only one data point for every minute was taken into account when calculating the goodness of fit for these experimental data sets.

The correct values presented here are mole or mass fraction in the actual mixture and the literature values for the pure compound saturation concentrations (Table 4~~3~~). However, the saturation concentration estimates obtained from the optimization process are effective saturation concentrations, because the evaporation models assume ideal behavior. Any non-ideal behavior of the mixtures will cause the estimated C_{sat} to differ from the literature values. The possible deviation from ideality of every mixture is assessed by performing AIOMFAC (http://www.aiomfac.caltech.edu, last accessed 11.01.2019, Zuend et al., 2008, 2011) calculations with the composition at the start of the evaporation as the input.

5.1 Evaporation of low viscosity~~non-viscous~~ mixtures

The correct mole fractions and saturation vapor pressures for the low viscosity~~non-viscous~~ mixtures 1 and 2 are listed in Table 4~~3~~ and shown for mixture 1 in Fig. 7 and for mixture 2 in Fig. 8. In both figures, two different MCGA estimates are shown. The darker squares represent optimization results where the literature values for ~~correct~~ molar masses and particle phase densit~~y~~ies were used. The light diamond markers represent optimization where the same molar mass and particle phase density ($M=200 \ g \ mol^{-1}$;~~-~~

$\rho = 1200$ kg m^{-3}) were used for every model compound. The vertical axis in Fig. 7 and Fig. 8 is mass fraction of a compound at the start of the evaporation since it is less sensitive to the assumed molar masses compared to mole fraction.

5.1.1 Mixture 1

485 The mass fraction estimates are close to the correct values for all the three compounds (Fig. 7). The correct value is within the uncertainty of the estimates for all the compounds except for the highest volatility compound (MCGA, exact compound properties) for which the 90th percentile corresponds to a mass fraction of approximately 0.28, 0.02 away from the correct value.

490 The saturation concentration estimates are slightly overestimated with both methods for the highest volatility compound (carbitol) and for the middle volatility compound (glycerol). For glycerol the MCGA estimate with correct literature properties (800 μg m^{-3}) is closer to the literature saturation concentration (370 μg m^{-3}, see Table 43 for references) than the MCGA estimate with equal compound properties (2100 μg m^{-3}). With equal compound properties for the estimates to produce comparable evaporation rates to measurements, a higher saturation concentration is needed to compensate for the

495 larger molar mass.

For the least volatile compound (PEG400), the estimated saturation concentrations show the larges variation. In fact, both estimates do not include the correct literature value in their distribution. This is again because of the low sensitivity of the evaporation curve to the least volatile compound. It does not make a significant difference to the overall goodness of fit if the

500 saturation concentration is 3 μg m^{-3} or 0.1 μg m^{-3} as in the time scales of the measurements all these saturation concentrations lead to practically no evaporation from the particle.

Figure S5a shows all the simulated and measured evaporation curves and Fig. 6a shows twenty best fit simulated evaporation curves and the measured one. The simulated curves show similar spread as with artificial data sets 1 and 2. In Fig. S5b the

505 correct literature values are used as input to the LLEVAP model and the resulting evaporation curve is compared with the measurements to show that with correct parameters from the literature and with correct mole fractions the model would produce evaporation rates similar to measurements everywhere except in the middle of the measurement where the simulated rate of evaporation is slower. This discrepancy could be explained by the non-ideality of the mixture as the AIOMFAC calculated activity coefficients are 1.12 and 1.88, respectively for carbitol and glycerol. Neglecting the non-ideality in the

510 model may have caused an overestimation of the saturation concentration of glycerol in the optimization.

5.1.2 Mixture 2

The estimated mass fractions and saturation concentrations for mixture 2 (Fig. 8) show different behaviour to the estimated properties of mixture 1. The only satisfactory estimates are the saturation concentration and mass fraction of the highest volatility compound (carbitol), for which both MCGA methods marginally overestimate the saturation concentration. The optimization performed with exact compound properties produces a mass fraction estimate that is 0.05 smaller than the correct value (0.30). In the MCGA runs with exact compound properties, the uncertainties are higher than in the MCGA runs with equal compound properties for all the compounds, especially in the saturation concentration estimate. The AIOMFAC calculations give an activity coefficient of 1.06 for carbitol which could explain some of the overestimation in the saturation concentration.

The estimates of the saturation concentrations and mass fractions for the two other compounds (malonic acid and PEG400) are problematic when compared with all of the other systems encountered so far. For both MCGA approaches the estimates clearly deviate from the values that were sought. The uncertainties of the estimated values with both approaches span over a wide range in the parameter space, from 0.03 to 0.66 in mass fraction and from 0.15 μg m^{-3} to almost 9500 μg m^{-3} in saturation concentration. The reason for this inaccuracy in the optimization method is discussed in Sect. 5.3.

5.2 Evaporation of high viscosity~~us~~ mixtures 3 and 4

Finally, the results concerning the evaporation of high viscosity~~us~~ mixtures 3 and 4 are described. For these optimization runs the correct molar masses, particle phase densities and gas phase diffusion coefficients were used for sucrose and glycerol. With both mixtures two different evaporation measurements were performed, one measured at high RH and one at lower RH. For the high RH case, it was assumed that the particles behave like well-mixed ideal liquids and, thus, the LLEVAP model was used to model the evaporation. For low RH measurements with significant particle phase diffusion limitations, KM-GAP was used to model the evaporation. The optimization to both relative humidities was performed simultaneously. In this case the goodness of fit was calculated as a sum of individual measurement-simulation MSEs.

Two restrictions were set for the new candidate creation. The candidate was not accepted if the overall particle viscosity was below 0.01 Pa s at the start of the evaporation. Such a low viscosity does not produce slower evaporation at low RH what is observed in the measurements and a low viscosity greatly increases the computation time of a single KM-GAP simulation. In addition, during the candidate creation, the free parameters were sorted based on the saturation concentrations. Effectively, this guides the optimization algorithm away from values that would produce wrong evaporation as the higher volatility compound (glycerol) was prevented to get associated with the preset properties of lower volatility compound (sucrose) (e.g. molar mass, gas phase diffusion coefficient) or vice versa. Ultimately the choice leads to a smaller number of iterations that must be calculated in order to get a reliable estimate for the free parameters.

The estimates for the saturation concentration of sucrose and glycerol and their mole fractions are shown in Fig. 9 for mixture 3 and in Fig. 10 for mixture 4. Table 65 shows the median and 10th and 90th percentiles of the estimated b_i factors with which the particle viscosity is calculated in the KM-GAP simulations. In addition, the spread of the simulations together with the measured evaporation of particles are reported in Fig. S7a (mixture 3) and Fig. S8a (mixture 4). In Fig. S7b and Fig. S8b, the KM-GAP and LLEVAP simulations made with the ~~correct~~ literature values are compared with the evaporation measurements. Figures 6c and 6d show the twenty best fit simulations together with the measured evaporation.

The saturation concentration of sucrose is presumably so low that practically no sucrose evaporates from the particle. For this reason, it is marked in Fig. 9 and Fig. 10 at the $C_{sat} = 1$ µg m^{-3} which was identified as the lower limit that can be reliably fitted considering the experimental timescale (see Sect. 4). The estimated saturation concentrations for sucrose are comparable to this value: for mixture 3 the estimated saturation concentrations are between 2-11 µg m^{-3} and for mixture 4 between 1-10 µg m^{-3}. The mole fraction estimates for sucrose are excellent as the deviation from the correct value is at maximum 0.02 for mixture 3 and 0.01 for mixture 4.

For the higher volatility compound glycerol, the optimization yields slightly lower saturation concentrations (200 – 285 µg m^{-3}) than the literature value (370 µg m^{-3}) for mixture 3. For mixture 4 the estimated saturation concentration matches the literature value better, although the literature value is at the high end of the estimated C_{sat} (260 – 380 µg m^{-3}). For the mole fraction of each compound at the start of the evaporation, the estimates are close to the real values.

Lastly, with mixtures 3 and 4 the contribution of each compound to the particle viscosity was estimated. If an ideal mixture is assumed, these contribution parameters (b_i in eq. (1)) can be compared to the pure compound viscosities. The estimated contribution parameters b together with pure component viscosity of sucrose and glycerol found from the literature, are shown in Table 65. For sucrose the estimated $b_{sucrose}$ values are on the lower end of the literature values and for glycerol the $b_{glycerol}$ estimates are several magnitudes smaller than the literature value.

5.3 Discussion on estimating the volatility and viscosity from EDB measurements

Overall, it can be said that the estimated properties are captured well when the process model optimization scheme is applied to real experiments. However, some aspects merit further discussion on the limitations of the method.

Among the ten artificial and experimental data sets considered in this work, the method fails to estimate the correct mass fractions at the start of the evaporation and the saturation concentrations only for malonic acid and PEG400 in mixture 2. This exception can be understood by looking at Fig. S6a. The measured evaporation curve is shaped like the letter L. There is a clear faster period of evaporation when mainly the highest volatility compound (carbitol) evaporates followed by evaporation of at least one other compound. If more than one compound characterized by low volatility is present (in this

case two, with $C_{sat} \approx 10$ µg m^{-3} or smaller) the evaporation curve will look the same as in the case of one low volatility
compound, i.e. the particle size remains practically constant towards the end, and it is difficult for an optimization algorithm
to distinguish between the two. This is an important finding because it provides information on the sensitivity of the model
to low volatility chemical species; in addition, it provides an estimate of what range in volatility can be accessible as a
function of the experimental timescale. When optimizing the LLEVAP model input to particles produced from mixture 2,
MCGA was set to find saturation concentrations and mass fractions for exactly three compounds. When one compound is
needed to produce the fast evaporation and one compound the slow evaporation the third compound is left over. In this case
MCGA finds solutions where the third compound's saturation concentration is close to either of the two other compounds or
its mass fraction at the start of the evaporation is insignificant. Fundamentally this result shows a limit to the optimization
method. If the properties of two compounds are close to each other so that they produce similar measurable quantity as they
would produce alone, the optimization method might not find a clearly defined estimate for these properties. This
shortcoming was encountered when finding optimal set of mass fractions and saturation concentrations for three compounds.
With artificial data set 4 it was shown that lumping 40 compounds to 6 volatility classes produced a good fit, meaning that
the impact of such shortcoming is expected to be limited when performing the optimization to "real" OA evaporation data
sets.

Another aspect concerns the lower estimate for the saturation concentration of glycerol compared to the ~~real~~literature value
and the estimated values for the b_i parameters of sucrose and glycerol. Fig. S7b and Fig. S8b show the simulated curves
when the real properties of the organics are used as input values. The simulated evaporation is faster than the measured one
which means that the properties estimated by optimizing model to match measured data are not expected to match with the
~~correct~~ literature values. AIOMFAC calculations give water activity coefficients of 0.50, 0.86 and 0.59 for mixture 3 at the
low and high RH and for mixture 4 at the low RH, respectively when using the start of the evaporation composition as input.
The activity coefficients for glycerol are all close to unity for these mixtures. Water activity coefficients smaller than unity
mean that the there is more water partitioned in the particle phase than calculated based on the ideality assumption. Due to
Raoult's law the rate of evaporation of glycerol might be hindered which might explain why the optimization method
underestimates glycerol's saturation concentration and why the literature values produce too fast evaporation when used as a
model input. AIOMFAC calculations produce a near unity (0.97) water activity coefficient for the high RH experiment of
mixture 4. With this experiment the AIOMFAC activity coefficient of glycerol is 0.68 which again might explain the
discrepancy.

When optimizing the viscosity, the overall particle viscosity is optimized which is made up of the individual contribution
parameters of sucrose and glycerol. These contribution parameters can be compared to the pure compound viscosities, if the
mixture is ideal. While at first the estimated b-parameters seem to be too high for sucrose and too low for glycerol, the range
of possible contribution parameter values allowed in the optimization was large, from 10^{-15} to 10^{20}. At a closer inspection of

19

the estimated b_i parameters (Fig. S9), it is clear that the high $b_{sucrose}$ are always associated with low $b_{glycerol}$ values. However, the literature values reported in Table 65 do not fit to the trend observed in Fig. S9. If the literature values were input to Eq. (1), they would produce higher viscosity than what is estimated with the process model optimization method. This discrepancy could be explained by the non-ideality of the mixtures 3 and 4 at low RH where AIOMFAC calculated activity coefficients for water were 0.50 and 0.59, respectively (i.e. there could be more water in the particle phase than what is calculated based on the ideality assumption). This additional water could decrease the particle phase viscosity.

6 Summary and conclusions

In this study, process model optimization methods were tested as a possible way of quantifying some of the physicochemical properties of organic aerosol particles that are challenging to measure directly. More specifically, the particle compounds' volatilities and particle viscosity were estimated by searching for those values that when used as an input to a detailed evaporation model produce an evaporation curve similar to the evaporation test data. Additionally, two different ways of stating the optimization problem were tested. Both the Monte Carlo Genetic Algorithm and Bayesian inference method yielded similar optimization results.

The process model optimization scheme was tested for both artificially generated and measured isothermal evaporation data. When fitting the model to artificial data, accurate estimates for both mole fraction and saturation concentrations of the components were obtained. With real experimental data the method produced good estimates given the fact that the models assumed ideal behavior and thermodynamic equilibrium calculations with AIOMFAC showed that the mixtures might be slightly non-ideal.

For some of the tested data sets, the few shortcomings of the method could be largely attributed to the fact that the model output was not sensitive to the changes in the estimated parameters with respect to the experimental timescale and parameter range. method can only characterize properties that influence the quantity that is measured. If some parameters are non-influential (or have a small influence over the observed timescales) to the model output or if the parameter is coupled to another parameter, they cannot be estimated precisely. This was the case with artificial data sets 3 and 4, in which the two least volatile compounds were almost interchangeable as both produce slow evaporation, and with the estimated viscosity of glycerol and sucrose in mixtures 3 and 4 where the b-parameters were coupled to produce the overall viscosity of the particle. This overall viscosity could be achieved by many combinations of the allowed values of the b-parameter in eq. (1).

In addition, if the estimated properties of two different compounds were close to each other the studied method might not be able to discriminate between them. This was observed with the evaporation of particles produced from mixture 2 as the

saturation concentrations of malonic acid and PEG400 were close to each other and produced nearly constant rates of
640   evaporation over the considered experimental timescale.

The process model optimization scheme does also depend on the process models that are used. If the model output with
~~correct~~ literature values deviates from the measurements, the obtained estimates will not be ~~correct~~exact. This kind of
drawback was encountered when estimating the saturation concentration of glycerol in evaporation of mixtures 3 and 4. This
645   can be the case if the model does not describe the system accurately, e.g. due to ignored non-ideality.

Optimizing process model input to match measured data is a promising method for the quantification of the volaility of OA
particle constituents and viscosity from evaporation experiments which are challenging properties to measure directly.
Further studies using this method should be accompanied with a clearly defined range of values for each estimated
650   parameter. This range should take into account what can be inferred from the data with respect to the experimental
conditions and model assumptions. Based on the analysis shown here, various parameters can be obtained from experimental
data using this method and the design of the experiments can be used to focus experiments on properties of interest. For
instance, in order to distinguish between saturation concentrations of low-volatile compounds, small particles and hours long
evaporation times are required. On the contrary, to distinguish between semivolatile or intermediate volatility compounds,
655   larger particles and/or high sampling time resolution for the short evaporation time scales are needed.

Author contributions: OPT developed the MCGA code with support from TY. VH and AL developed the BI code with
support from KL. OPT, TY and KL designed the simulations and OPT and VH performed them. GR and JR designed and
performed the measurements. All authors participated in the interpretation of the data. OPT prepared the manuscript with
665   contributions from all co-authors.

Competing interests: The authors declare that they have no conflict of interest.

21

References

Abramson, E., Imre, D., Beránek, J., Wilson, J. and Zelenyuk, A.: Experimental determination of chemical diffusion within secondary organic aerosol particles, Phys. Chem. Chem. Phys., 15(8), 2983–2991, doi:10.1039/C2CP44013J, 2013.

Arangio, A. M., Slade, J. H., Berkemeier, T., Pöschl, U., Knopf, D. A. and Shiraiwa, M.: Multiphase Chemical Kinetics of OH Radical Uptake by Molecular Organic Markers of Biomass Burning Aerosols: Humidity and Temperature Dependence, Surface Reaction, and Bulk Diffusion, J. Phys. Chem. A, 119(19), 4533–4544, doi:10.1021/jp510489z, 2015.

Bayes, T., Price, R. and Canton, J.: An essay towards solving a problem in the doctrine of chances, 1763.

Berkemeier, T., S. Steimer, S., K. Krieger, U., Peter, T., Pöschl, U., Ammann, M. and Shiraiwa, M.: Ozone uptake on glassy, semi-solid and liquid organic matter and the role of reactive oxygen intermediates in atmospheric aerosol chemistry, Phys. Chem. Chem. Phys., 18(18), 12662–12674, doi:10.1039/C6CP00634E, 2016.

Berkemeier, T., Ammann, M., Krieger, U. K., Peter, T., Spichtinger, P., Pöschl, U., Shiraiwa, M. and Huisman, A. J.: Technical note: Monte Carlo genetic algorithm (MCGA) for model analysis of multiphase chemical kinetics to determine transport and reaction rate coefficients using multiple experimental data sets, Atmospheric Chem. Phys., 17(12), 8021–8029, doi:10.5194/acp-17-8021-2017, 2017.

Bilde, M., Barsanti, K., Booth, M., Cappa, C. D., Donahue, N. M., Emanuelsson, E. U., McFiggans, G., Krieger, U. K., Marcolli, C., Topping, D., Ziemann, P., Barley, M., Clegg, S., Dennis-Smither, B., Hallquist, M., Hallquist, \AAsa M., Khlystov, A., Kulmala, M., Mogensen, D., Percival, C. J., Pope, F., Reid, J. P., V Ribeiro da Silva, M. A., Rosenoern, T., Salo, K., Pia Soonsin, V., Yli-Juuti, T., Prisle, N. L., Pagels, J., Rarey, J., Zardini, A. A. and Riipinen, I.: Saturation Vapor Pressures and Transition Enthalpies of Low- Volatility Organic Molecules of Atmospheric Relevance: From Dicarboxylic Acids to Complex Mixtures, Chem Rev, 115, 4115–4156, doi:10.1021/cr5005502, 2015.

Carpenter, B., Gelman, A., Hoffman, M. D., Lee, D., Goodrich, B., Betancourt, M., Brubaker, M., Guo, J., Li, P. and Riddell, A.: Stan: A probabilistic programming language, J. Stat. Softw., 76(1), 2017.

Davies, J. F., Haddrell, A. E. and Reid, J. P.: Time-Resolved Measurements of the Evaporation of Volatile Components from Single Aerosol Droplets, Aerosol Sci. Technol., 46(6), 666–677, doi:10.1080/02786826.2011.652750, 2012.

Davies, J. F., Haddrell, A. E., Rickards, A. M. J. and Reid, J. P.: Simultaneous Analysis of the Equilibrium Hygroscopicity and Water Transport Kinetics of Liquid Aerosol, Anal. Chem., 85(12), 5819–5826, doi:10.1021/ac4005502, 2013.

Donahue, N. M., Robinson, a. L., Stanier, C. O. and Pandis, S. N.: Coupled partitioning, dilution, and chemical aging of semivolatile organics, Environ. Sci. Technol., 40(8), 2635–2643, doi:10.1021/es052297c, 2006.

Einstein, A.: Über die von der molekularkinetischen Theorie der Wärme geforderte Bewegung von in ruhenden Flüssigkeiten suspendierten Teilchen, Ann. Phys., 322(8), 549–560, doi:10.1002/andp.19053220806, 1905.

Gelman, A., Stern, H. S., Carlin, J. B., Dunson, D. B., Vehtari, A. and Rubin, D. B.: Bayesian data analysis, Chapman and Hall/CRC., 2013.

Glantschnig, W. J. and Chen, S.-H.: Light scattering from water droplets in the geometrical optics approximation, Appl. Opt., 20(14), 2499, doi:10.1364/AO.20.002499, 1981.

Hallquist, M., Wenger, J. C., Baltensperger, U., Rudich, Y., Simpson, D., Claeys, M., Dommen, J., Donahue, N. M., George, C., Goldstein, A. H., Hamilton, J. F., Herrmann, H., Hoffmann, T., Iinuma, Y., Jang, M., Jenkin, M. E., Jimenez, J. L., Kiendler-Scharr, A., Maenhaut, W., McFiggans, G., Mentel, Th. F., Monod, A., Prévôt, A. S. H., Seinfeld, J. H., Surratt, J. D., Szmigielski, R. and Wildt, J.: The formation, properties and impact of secondary organic aerosol: current and emerging issues, Atmos Chem Phys, 9(14), 5155–5236, doi:10.5194/acp-9-5155-2009, 2009.

Haynes, W. M.: CRC handbook of chemistry and physics, 6th ed., CRC press., 2009.

Hernández, W. P., Castello, D. A., Roitman, N. and Magluta, C.: Thermorheologically simple materials: A bayesian framework for model calibration and validation, J. Sound Vib., 402, 14–30, doi:10.1016/j.jsv.2017.05.005, 2017.

Hoffman, M. D. and Gelman, A.: The No-U-turn sampler: adaptively setting path lengths in Hamiltonian Monte Carlo., J. Mach. Learn. Res., 15(1), 1593–1623, 2014.

Jimenez, J. L., Canagaratna, M. R., Donahue, N. M., Prevot, A. S. H., Zhang, Q., Kroll, J. H., DeCarlo, P. F., Allan, J. D., Coe, H., Ng, N. L., Aiken, A. C., Docherty, K. S., Ulbrich, I. M., Grieshop, A. P., Robinson, A. L., Duplissy, J., Smith, J. D., Wilson, K. R., Lanz, V. A., Hueglin, C., Sun, Y. L., Tian, J., Laaksonen, A., Raatikainen, T., Rautiainen, J., Vaattovaara, P., Ehn, M., Kulmala, M., Tomlinson, J. M., Collins, D. R., Cubison, M. J., Dunlea, E. J., Huffman, J. A., Onasch, T. B., Alfarra, M. R., Williams, P. I., Bower, K., Kondo, Y., Schneider, J., Drewnick, F., Borrmann, S., Weimer, S., Demerjian, K., Salcedo, D., Cottrell, L., Griffin, R., Takami, A., Miyoshi, T., Hatakeyama, S., Shimono, A., Sun, J. Y., Zhang, Y. M., Dzepina, K., Kimmel, J. R., Sueper, D., Jayne, J. T., Herndon, S. C., Trimborn, A. M., Williams, L. R., Wood, E. C., Middlebrook, A. M., Kolb, C. E., Baltensperger, U., Worsnop, D. R. and Worsnop, D. R.: Evolution of organic aerosols in the atmosphere., Science, 326(5959), 1525–9, doi:10.1126/science.1180353, 2009.

Kaipio, J. P., Kolehmainen, V., Somersalo, E. and Vauhkonen, M.: Statistical inversion and Monte Carlo sampling methods in electrical impedance tomography, Inverse Probl., 16(5), 1487, doi:10.1088/0266-5611/16/5/321, 2000.

Kanakidou, M., Seinfeld, J. H., Pandis, S. N., Barnes, I., Dentener, F. J., Facchini, M. C., Dingenen, R. V., Ervens, B., Nenes, A., Nielsen, C. J., Swietlicki, E., Putaud, J. P., Balkanski, Y., Fuzzi, S., Horth, J., Moortgat, G. K., Winterhalter, R., Myhre, C. E. L., Tsigaridis, K., Vignati, E., Stephanou, E. G. and Wilson, J.: Organic aerosol and global climate modelling: a review, Atmos Chem Phys, 71, 2005.

Krieger, U. K., Siegrist, F., Marcolli, C., Emanuelsson, E. U., Gøbel, F. M., Bilde, M., Marsh, A., Reid, J. P., Huisman, A. J., Riipinen, I., Hyttinen, N., Myllys, N., Kurtén, T., Bannan, T., Percival, C. J. and Topping, D.: A reference data set for validating vapor pressure measurement techniques: homologous series of polyethylene glycols, Atmospheric Meas. Tech., 11(1), 49–63, doi:https://doi.org/10.5194/amt-11-49-2018, 2018.

Kulmala, M., Vesala, T. and Wagner, P. E.: An analytical expression for the rate of binary condensational particle growth, Proc R Soc Lond A, 441(1913), 589–605, doi:10.1098/rspa.1993.0081, 1993.

Kulmala, M., Vesala, T., Schwarz, J. and Smolik, J.: Mass transfer from a drop—II. Theoretical analysis of temperature dependent mass flux correlation, Int. J. Heat Mass Transf., 38(9), 1705–1708, doi:10.1016/0017-9310(94)00302-C, 1995.

Lehtinen, K. E. J. and Kulmala, M.: A model for particle formation and growth in the atmosphere with molecular resolution in size, Atmos Chem Phys, 7, 2003.

Liu, P., Li, Y. J., Wang, Y., Gilles, M. K., Zaveri, R. A., Bertram, A. K. and Martin, S. T.: Lability of secondary organic particulate matter., Proc. Natl. Acad. Sci. U. S. A., 113(45), 12643–12648, doi:10.1073/pnas.1603138113, 2016.

Lowe, S., Partridge, D. G., Topping, D. and Stier, P.: Inverse modelling of Köhler theory – Part 1: A response surface analysis of CCN spectra with respect to surface-active organic species, Atmospheric Chem. Phys., 16(17), 10941–10963, doi:https://doi.org/10.5194/acp-16-10941-2016, 2016.

Marsh, A., Miles, R. E. H., Rovelli, G., Cowling, A. G., Nandy, L., Dutcher, C. S. and Reid, J. P.: Influence of organic compound functionality on aerosol hygroscopicity: dicarboxylic acids, alkyl-substituents, sugars and amino acids, Atmospheric Chem. Phys., 17(9), 5583–5599, doi:10.5194/acp-17-5583-2017, 2017.

Metropolis, N., Rosenbluth, A. W., Rosenbluth, M. N., Teller, A. H. and Teller, E.: Equation of State Calculations by Fast Computing Machines, J. Chem. Phys., 21(6), 1087–1092, doi:10.1063/1.1699114, 1953.

O'Meara, S., Topping, D. O. and McFiggans, G.: The rate of equilibration of viscous aerosol particles, Atmospheric Chem. Phys., 16(8), 5299–5313, doi:10.5194/acp-16-5299-2016, 2016.

Pajunoja, A., Lambe, A. T., Hakala, J., Rastak, N., Cummings, M. J., Brogan, J. F., Hao, L., Paramonov, M., Hong, J., Prisle, N. L., Malila, J., Romakkaniemi, S., Lehtinen, K. E. J., Laaksonen, A., Kulmala, M., Massoli, P., Onasch, T. B., Donahue, N. M., Riipinen, I., Davidovits, P., Worsnop, D. R., Petäjä, T. and Virtanen, A.: Adsorptive uptake of water by semisolid secondary organic aerosols, Geophys. Res. Lett., 42(8), 3063–3068, doi:10.1002/2015GL063142, 2015.

Power, R. M., Simpson, S. H., Reid, J. P. and Hudson, A. J.: The transition from liquid to solid-like behaviour in ultrahigh viscosity aerosol particles, Chem. Sci., 4(6), 2597, doi:10.1039/c3sc50682g, 2013.

Reid, J. P., Bertram, A. K., Topping, D. O., Laskin, A., Martin, S. T., Petters, M. D., Pope, F. D. and Rovelli, G.: The viscosity of atmospherically relevant organic particles, Nat. Commun., 9(1), 956, doi:10.1038/s41467-018-03027-z, 2018.

Reid, R. C., Prausnitz, J. M. and Poling, B. E.: The properties of gases and liquids, 1987.

Renbaum-Wolff, L., Grayson, J. W., Bateman, A. P., Kuwata, M., Sellier, M., Murray, B. J., Shilling, J. E., Martin, S. T. and Bertram, A. K.: Viscosity of α-pinene secondary organic material and implications for particle growth and reactivity, Proc. Natl. Acad. Sci., 110(20), 8014–8019, doi:10.1073/pnas.1219548110, 2013.

Rovelli, G., Miles, R. E. H., Reid, J. P. and Clegg, S. L.: Accurate Measurements of Aerosol Hygroscopic Growth over a Wide Range in Relative Humidity, J. Phys. Chem. A, 120(25), 4376–4388, doi:10.1021/acs.jpca.6b04194, 2016.

Rumble, J., R., Lide, D., R. and Bruno, T., J.: CRC handbook of chemistry and physics, 99th ed., 99th ed., CRC press, Taylor & Francis Group, Boca Raton, FL., 2018.

Shiraiwa, M., Pfrang, C., Koop, T. and Pöschl, U.: Kinetic multi-layer model of gas-particle interactions in aerosols and clouds (KM-GAP): linking condensation, evaporation and chemical reactions of organics, oxidants and water, Atmospheric Chem. Phys., 12(5), 2777–2794, doi:10.5194/acp-12-2777-2012, 2012.

Shiraiwa, M., Zuend, A., Bertram, A. K. and Seinfeld, J. H.: Gas–particle partitioning of atmospheric aerosols: interplay of physical state, non-ideal mixing and morphology, Phys. Chem. Chem. Phys., 15(27), 11441, doi:10.1039/c3cp51595h, 2013.

Shiraiwa, M., Li, Y., Tsimpidi, A. P., Karydis, V. A., Berkemeier, T., Pandis, S. N., Lelieveld, J., Koop, T. and Pöschl, U.: Global distribution of particle phase state in atmospheric secondary organic aerosols, Nat. Commun., 8, 15002, doi:10.1038/ncomms15002, 2017.

Song, Y. C., Haddrell, A. E., Bzdek, B. R., Reid, J. P., Bannan, T., Topping, D. O., Percival, C. and Cai, C.: Measurements and Predictions of Binary Component Aerosol Particle Viscosity, J. Phys. Chem. A, 120(41), 8123–8137, doi:10.1021/acs.jpca.6b07835, 2016.

Tsigaridis, K., Daskalakis, N., Kanakidou, M., Adams, P. J., Artaxo, P., Bahadur, R., Balkanski, Y., Bauer, S. E., Bellouin, N., Benedetti, A., Bergman, T., Berntsen, T. K., Beukes, J. P., Bian, H., Carslaw, K. S., Chin, M., Curci, G., Diehl, T., Easter, R. C., Ghan, S. J., Gong, S. L., Hodzic, A., Hoyle, C. R., Iversen, T., Jathar, S., Jimenez, J. L., Kaiser, J. W., Kirkevåg, A., Koch, D., Kokkola, H., Lee, Y. H., Lin, G., Liu, X., Luo, G., Ma, X., Mann, G. W., Mihalopoulos, N., Morcrette, J.-J., Müller, J.-F., Myhre, G., Myriokefalitakis, S., Ng, N. L., O'Donnell, D., Penner, J. E., Pozzoli, L., Pringle, K. J., Russell, L. M., Schulz, M., Sciare, J., Seland, Ø., Shindell, D. T., Sillman, S., Skeie, R. B., Spracklen, D., Stavrakou, T., Steenrod, S. D., Takemura, T., Tiitta, P., Tilmes, S., Tost, H., van Noije, T., van Zyl, P. G., von Salzen, K., Yu, F., Wang, Z., Wang, Z., Zaveri, R. A., Zhang, H., Zhang, K., Zhang, Q. and Zhang, X.: The AeroCom evaluation and intercomparison of organic aerosol in global models, Atmospheric Chem. Phys., 14(19), 10845–10895, doi:https://doi.org/10.5194/acp-14-10845-2014, 2014.

Vaden, T. D., Imre, D., Beránek, J., Shrivastava, M. and Zelenyuk, A.: (suppl.)Evaporation kinetics and phase of laboratory and ambient secondary organic aerosol., Proc. Natl. Acad. Sci. U. S. A., 108(6), 2190–2195, doi:10.1073/pnas.1013391108, 2011.

Varvia, P., Rautiainen, M. and Seppänen, A.: Bayesian estimation of seasonal course of canopy leaf area index from hyperspectral satellite data, J. Quant. Spectrosc. Radiat. Transf., 208, 19–28, doi:10.1016/j.jqsrt.2018.01.008, 2018.

Vesala, T., Kulmala, M., Rudolf, R., Vrtala, A. and Wagner, P. E.: Models for condensational growth and evaporation of binary aerosol particles, J. Aerosol Sci., 28(4), 565–598, doi:10.1016/S0021-8502(96)00461-2, 1997.

Virtanen, A., Joutsensaari, J., Koop, T., Kannosto, J., Yli-Pirilä, P., Leskinen, J., Mäkelä, J. M., Holopainen, J. K., Pöschl, U., Kulmala, M., Worsnop, D. R. and Laaksonen, A.: An amorphous solid state of biogenic secondary organic aerosol particles, Nature, 467(7317), 824–827, doi:10.1038/nature09455, 2010.

Wilson, J., Imre, D., Beraek, J., Shrivastava, M. and Zelenyuk, A.: Evaporation Kinetics of Laboratory-Generated Secondary Organic Aerosols at Elevated Relative Humidity, , doi:10.1021/es505331d, 2015.

Yli-Juuti, T., Pajunoja, A., Tikkanen, O.-P., Buchholz, A., Faiola, C., Väisänen, O., Hao, L., Kari, E., Peräkylä, O., Garmash, O., Shiraiwa, M., Ehn, M., Lehtinen, K. and Virtanen, A.: Factors controlling the evaporation of secondary organic aerosol from α-pinene ozonolysis, Geophys. Res. Lett., 44(5), 2016GL072364, doi:10.1002/2016GL072364, 2017.

Zuend, A., Marcolli, C., Luo, B. P. and Peter, T.: A thermodynamic model of mixed organic-inorganic aerosols to predict activity coefficients, Atmospheric Chem. Phys., 8(16), 4559–4593, doi:https://doi.org/10.5194/acp-8-4559-2008, 2008.

Zuend, A., Marcolli, C., Booth, A. M., Lienhard, D. M., Soonsin, V., Krieger, U. K., Topping, D. O., McFiggans, G., Peter, T. and Seinfeld, J. H.: New and extended parameterization of the thermodynamic model AIOMFAC: calculation of activity coefficients for organic-inorganic mixtures containing carboxyl, hydroxyl, carbonyl, ether, ester, alkenyl, alkyl, and aromatic functional groups, Atmospheric Chem. Phys., 11(17), 9155–9206, doi:https://doi.org/10.5194/acp-11-9155-2011,

2011.Abramson, E., Imre, D., Beránek, J., Wilson, J. and Zelenyuk, A.: Experimental determination of chemical diffusion within secondary organic aerosol particles, Phys. Chem. Chem. Phys., 15(8), 2983–2991, doi:10.1039/C2CP44013J, 2013.

Arangio, A. M., Slade, J. H., Berkemeier, T., Pöschl, U., Knopf, D. A. and Shiraiwa, M.: Multiphase Chemical Kinetics of OH Radical Uptake by Molecular Organic Markers of Biomass Burning Aerosols: Humidity and Temperature Dependence, Surface Reaction, and Bulk Diffusion, J. Phys. Chem. A, 119(19), 4533–4544, doi:10.1021/jp510489z, 2015.

Bayes, T., Price, R. and Canton, J.: An essay towards solving a problem in the doctrine of chances, 1763.

Berkemeier, T., S. Steimer, S., K. Krieger, U., Peter, T., Pöschl, U., Ammann, M. and Shiraiwa, M.: Ozone uptake on glassy, semi-solid and liquid organic matter and the role of reactive oxygen intermediates in atmospheric aerosol chemistry, Phys. Chem. Chem. Phys., 18(18), 12662–12674, doi:10.1039/C6CP00634E, 2016.

Berkemeier, T., Ammann, M., Krieger, U. K., Peter, T., Spichtinger, P., Pöschl, U., Shiraiwa, M. and Huisman, A. J.: Technical note: Monte Carlo genetic algorithm (MCGA) for model analysis of multiphase chemical kinetics to determine transport and reaction rate coefficients using multiple experimental data sets, Atmospheric Chem. Phys., 17(12), 8021–8029, doi:10.5194/acp-17-8021-2017, 2017.

Bilde, M., Barsanti, K., Booth, M., Cappa, C. D., Donahue, N. M., Emanuelsson, E. U., McFiggans, G., Krieger, U. K., Marcolli, C., Topping, D., Ziemann, P., Barley, M., Clegg, S., Dennis-Smither, B., Hallquist, M., Hallquist, \AAsa M, Khlystov, A., Kulmala, M., Mogensen, D., Percival, C. J., Pope, F., Reid, J. P., V Ribeiro da Silva, M. A., Rosenoern, T., Salo, K., Pia Soonsin, V., Yli-Juuti, T., Prisle, N. L., Pagels, J., Rarey, J., Zardini, A. A. and Riipinen, I.: Saturation Vapor Pressures and Transition Enthalpies of Low- Volatility Organic Molecules of Atmospheric Relevance: From Dicarboxylic Acids to Complex Mixtures, Chem Rev, 115, 4115–4156, doi:10.1021/cr5005502, 2015.

Carpenter, B., Gelman, A., Hoffman, M. D., Lee, D., Goodrich, B., Betancourt, M., Brubaker, M., Guo, J., Li, P. and Riddell, A.: Stan: A probabilistic programming language, J. Stat. Softw., 76(1), 2017.

Davies, J. F., Haddrell, A. E. and Reid, J. P.: Time-Resolved Measurements of the Evaporation of Volatile Components from Single Aerosol Droplets, Aerosol Sci. Technol., 46(6), 666–677, doi:10.1080/02786826.2011.652750, 2012.

Davies, J. F., Haddrell, A. E., Rickards, A. M. J. and Reid, J. P.: Simultaneous Analysis of the Equilibrium Hygroscopicity and Water Transport Kinetics of Liquid Aerosol, Anal. Chem., 85(12), 5819–5826, doi:10.1021/ac4005502, 2013.

Donahue, N. M., Robinson, a. L., Stanier, C. O. and Pandis, S. N.: Coupled partitioning, dilution, and chemical aging of semivolatile organics, Environ. Sci. Technol., 40(8), 2635–2643, doi:10.1021/es052297c, 2006.

Einstein, A.: Über die von der molekularkinetischen Theorie der Wärme geforderte Bewegung von in ruhenden Flüssigkeiten suspendierten Teilchen, Ann. Phys., 322(8), 549–560, doi:10.1002/andp.19053220806, 1905.

Gelman, A., Stern, H. S., Carlin, J. B., Dunson, D. B., Vehtari, A. and Rubin, D. B.: Bayesian data analysis, Chapman and Hall/CRC., 2013.

Glantschnig, W. J. and Chen, S.-H.: Light scattering from water droplets in the geometrical optics approximation, Appl. Opt., 20(14), 2499, doi:10.1364/AO.20.002499, 1981.

Hallquist, M., Wenger, J. C., Baltensperger, U., Rudich, Y., Simpson, D., Claeys, M., Dommen, J., Donahue, N. M., George, C., Goldstein, A. H., Hamilton, J. F., Herrmann, H., Hoffmann, T., Iinuma, Y., Jang, M., Jenkin, M. E., Jimenez, J. L., Kiendler-Scharr, A., Maenhaut, W., McFiggans, G., Mentel, Th. F., Monod, A., Prévôt, A. S. H., Seinfeld, J. H., Surratt, J. D., Szmigielski, R. and Wildt, J.: The formation, properties and impact of secondary organic aerosol: current and emerging issues, Atmos Chem Phys, 9(14), 5155–5236, doi:10.5194/acp-9-5155-2009, 2009.

Haynes, W. M.: CRC handbook of chemistry and physics, 6th ed., CRC press., 2009.

Hernández, W. P., Castello, D. A., Roitman, N. and Magluta, C.: Thermorheologically simple materials: A bayesian framework for model calibration and validation, J. Sound Vib., 402, 14–30, doi:10.1016/j.jsv.2017.05.005, 2017.

Hoffman, M. D. and Gelman, A.: The No-U-turn sampler: adaptively setting path lengths in Hamiltonian Monte Carlo., J. Mach. Learn. Res., 15(1), 1593–1623, 2014.

Jimenez, J. L., Canagaratna, M. R., Donahue, N. M., Prevot, A. S. H., Zhang, Q., Kroll, J. H., DeCarlo, P. F., Allan, J. D., Coe, H., Ng, N. L., Aiken, A. C., Docherty, K. S., Ulbrich, I. M., Grieshop, A. P., Robinson, A. L., Duplissy, J., Smith, J. D., Wilson, K. R., Lanz, V. A., Hueglin, C., Sun, Y. L., Tian, J., Laaksonen, A., Raatikainen, T., Rautiainen, J., Vaattovaara, P., Ehn, M., Kulmala, M., Tomlinson, J. M., Collins, D. R., Cubison, M. J., Dunlea, E. J., Huffman, J. A., Onasch, T. B., Alfarra, M. R., Williams, P. I., Bower, K., Kondo, Y., Schneider, J., Drewnick, F., Borrmann, S., Weimer, S., Demerjian, K., Salcedo, D., Cottrell, L., Griffin, R., Takami, A., Miyoshi, T., Hatakeyama, S., Shimono, A., Sun, J. Y., Zhang, Y. M., Dzepina, K., Kimmel, J. R., Sueper, D., Jayne, J. T., Herndon, S. C., Trimborn, A. M., Williams, L. R., Wood, E. C., Middlebrook, A. M., Kolb, C. E., Baltensperger, U., Worsnop, D. R. and Worsnop, D. R.: Evolution of organic aerosols in the atmosphere., Science, 326(5959), 1525–9, doi:10.1126/science.1180353, 2009.

Kaipio, J. P., Kolehmainen, V., Somersalo, E. and Vauhkonen, M.: Statistical inversion and Monte Carlo sampling methods in electrical impedance tomography, Inverse Probl., 16(5), 1487, doi:10.1088/0266-5611/16/5/321, 2000.

Kanakidou, M., Seinfeld, J. H., Pandis, S. N., Barnes, I., Dentener, F. J., Facchini, M. C., Dingenen, R. V., Ervens, B., Nenes, A., Nielsen, C. J., Swietlicki, E., Putaud, J. P., Balkanski, Y., Fuzzi, S., Horth, J., Moortgat, G. K., Winterhalter, R., Myhre, C. E. L., Tsigaridis, K., Vignati, E., Stephanou, E. G. and Wilson, J.: Organic aerosol and global climate modelling: a review, Atmos Chem Phys, 71, 2005.

Krieger, U. K., Siegrist, F., Marcolli, C., Emanuelsson, E. U., Gøbel, F. M., Bilde, M., Marsh, A., Reid, J. P., Huisman, A. J., Riipinen, I., Hyttinen, N., Myllys, N., Kurtén, T., Bannan, T., Percival, C. J. and Topping, D.: A reference data set for validating vapor pressure measurement techniques: homologous series of polyethylene glycols, Atmospheric Meas. Tech., 11(1), 49–63, doi:https://doi.org/10.5194/amt-11-49-2018, 2018.

Kulmala, M., Vesala, T. and Wagner, P. E.: An analytical expression for the rate of binary condensational particle growth, Proc R Soc Lond A, 441(1913), 589–605, doi:10.1098/rspa.1993.0081, 1993.

Kulmala, M., Vesala, T., Schwarz, J. and Smolik, J.: Mass transfer from a drop—II. Theoretical analysis of temperature dependent mass flux correlation, Int. J. Heat Mass Transf., 38(9), 1705–1708, doi:10.1016/0017-9310(94)00302-C, 1995.

27

Lehtinen, K. E. J. and Kulmala, M.: A model for particle formation and growth in the atmosphere with molecular resolution in size, Atmos Chem Phys, 7, 2003.

Liu, P., Li, Y. J., Wang, Y., Gilles, M. K., Zaveri, R. A., Bertram, A. K. and Martin, S. T.: Lability of secondary organic particulate matter., Proc. Natl. Acad. Sci. U. S. A., 113(45), 12643–12648, doi:10.1073/pnas.1603138113, 2016.

Marsh, A., Miles, R. E. H., Rovelli, G., Cowling, A. G., Nandy, L., Dutcher, C. S. and Reid, J. P.: Influence of organic compound functionality on aerosol hygroscopicity: dicarboxylic acids, alkyl-substituents, sugars and amino acids, Atmospheric Chem. Phys., 17(9), 5583–5599, doi:10.5194/acp-17-5583-2017, 2017.

Metropolis, N., Rosenbluth, A. W., Rosenbluth, M. N., Teller, A. H. and Teller, E.: Equation of State Calculations by Fast Computing Machines, J. Chem. Phys., 21(6), 1087–1092, doi:10.1063/1.1699114, 1953.

O'Meara, S., Topping, D. O. and McFiggans, G.: The rate of equilibration of viscous aerosol particles, Atmospheric Chem. Phys., 16(8), 5299–5313, doi:10.5194/acp-16-5299-2016, 2016.

Pajunoja, A., Lambe, A. T., Hakala, J., Rastak, N., Cummings, M. J., Brogan, J. F., Hao, L., Paramonov, M., Hong, J., Prisle, N. L., Malila, J., Romakkaniemi, S., Lehtinen, K. E. J., Laaksonen, A., Kulmala, M., Massoli, P., Onasch, T. B., Donahue, N. M., Riipinen, I., Davidovits, P., Worsnop, D. R., Petäjä, T. and Virtanen, A.: Adsorptive uptake of water by semisolid secondary organic aerosols, Geophys. Res. Lett., 42(8), 3063–3068, doi:10.1002/2015GL063142, 2015.

Power, R. M., Simpson, S. H., Reid, J. P. and Hudson, A. J.: The transition from liquid to solid-like behaviour in ultrahigh viscosity aerosol particles, Chem. Sci., 4(6), 2597, doi:10.1039/c3sc50682g, 2013.

Reid, J. P., Bertram, A. K., Topping, D. O., Laskin, A., Martin, S. T., Petters, M. D., Pope, F. D. and Rovelli, G.: The viscosity of atmospherically relevant organic particles, Nat. Commun., 9(1), 956, doi:10.1038/s41467-018-03027-z, 2018.

Reid, R. C., Prausnitz, J. M. and Poling, B. E.: The properties of gases and liquids, 1987.

Renbaum-Wolff, L., Grayson, J. W., Bateman, A. P., Kuwata, M., Sellier, M., Murray, B. J., Shilling, J. E., Martin, S. T. and Bertram, A. K.: Viscosity of α-pinene secondary organic material and implications for particle growth and reactivity, Proc. Natl. Acad. Sci., 110(20), 8014–8019, doi:10.1073/pnas.1219548110, 2013.

Rovelli, G., Miles, R. E. H., Reid, J. P. and Clegg, S. L.: Accurate Measurements of Aerosol Hygroscopic Growth over a Wide Range in Relative Humidity, J. Phys. Chem. A, 120(25), 4376–4388, doi:10.1021/acs.jpca.6b04194, 2016.

Rumble, J., R., Lide, D., R. and Bruno, T., J.: CRC handbook of chemistry and physics, 99th ed., 99th ed., CRC press, Taylor & Francis Group, Boca Raton, FL., 2018.

Shiraiwa, M., Pfrang, C., Koop, T. and Pöschl, U.: Kinetic multi-layer model of gas-particle interactions in aerosols and clouds (KM-GAP): linking condensation, evaporation and chemical reactions of organics, oxidants and water, Atmospheric Chem. Phys., 12(5), 2777–2794, doi:10.5194/acp-12-2777-2012, 2012.

Shiraiwa, M., Zuend, A., Bertram, A. K. and Seinfeld, J. H.: Gas–particle partitioning of atmospheric aerosols: interplay of physical state, non-ideal mixing and morphology, Phys. Chem. Chem. Phys., 15(27), 11441, doi:10.1039/c3cp51595h, 2013.

Shiraiwa, M., Li, Y., Tsimpidi, A. P., Karydis, V. A., Berkemeier, T., Pandis, S. N., Lelieveld, J., Koop, T. and Pöschl, U.: Global distribution of particle phase state in atmospheric secondary organic aerosols, Nat. Commun., 8, 15002, doi:10.1038/ncomms15002, 2017.

Song, Y. C., Haddrell, A. E., Bzdek, B. R., Reid, J. P., Bannan, T., Topping, D. O., Percival, C. and Cai, C.: Measurements and Predictions of Binary Component Aerosol Particle Viscosity, J. Phys. Chem. A, 120(41), 8123–8137, doi:10.1021/acs.jpca.6b07835, 2016.

Tsigaridis, K., Daskalakis, N., Kanakidou, M., Adams, P. J., Artaxo, P., Bahadur, R., Balkanski, Y., Bauer, S. E., Bellouin, N., Benedetti, A., Bergman, T., Berntsen, T. K., Beukes, J. P., Bian, H., Carslaw, K. S., Chin, M., Curci, G., Diehl, T., Easter, R. C., Ghan, S. J., Gong, S. L., Hodzic, A., Hoyle, C. R., Iversen, T., Jathar, S., Jimenez, J. L., Kaiser, J. W., Kirkevåg, A., Koch, D., Kokkola, H., Lee, Y. H., Lin, G., Liu, X., Luo, G., Ma, X., Mann, G. W., Mihalopoulos, N., Morcrette, J.-J., Müller, J.-F., Myhre, G., Myriokefalitakis, S., Ng, N. L., O'Donnell, D., Penner, J. E., Pozzoli, L., Pringle, K. J., Russell, L. M., Schulz, M., Sciare, J., Seland, Ø., Shindell, D. T., Sillman, S., Skeie, R. B., Spracklen, D., Stavrakou, T., Steenrod, S. D., Takemura, T., Tiitta, P., Tilmes, S., Tost, H., van Noije, T., van Zyl, P. G., von Salzen, K., Yu, F., Wang, Z., Wang, Z., Zaveri, R. A., Zhang, H., Zhang, K., Zhang, Q. and Zhang, X.: The AeroCom evaluation and intercomparison of organic aerosol in global models, Atmospheric Chem. Phys., 14(19), 10845–10895, doi:https://doi.org/10.5194/acp-14-10845-2014, 2014.

Vaden, T. D., Imre, D., Beránek, J., Shrivastava, M. and Zelenyuk, A.: (suppl.)Evaporation kinetics and phase of laboratory and ambient secondary organic aerosol., Proc. Natl. Acad. Sci. U. S. A., 108(6), 2190–2195, doi:10.1073/pnas.1013391108, 2011.

Varvia, P., Rautiainen, M. and Seppänen, A.: Bayesian estimation of seasonal course of canopy leaf area index from hyperspectral satellite data, J. Quant. Spectrosc. Radiat. Transf., 208, 19–28, doi:10.1016/j.jqsrt.2018.01.008, 2018.

Vesala, T., Kulmala, M., Rudolf, R., Vrtala, A. and Wagner, P. E.: Models for condensational growth and evaporation of binary aerosol particles, J. Aerosol Sci., 28(4), 565–598, doi:10.1016/S0021-8502(96)00461-2, 1997.

Virtanen, A., Joutsensaari, J., Koop, T., Kannosto, J., Yli-Pirilä, P., Leskinen, J., Mäkelä, J. M., Holopainen, J. K., Pöschl, U., Kulmala, M., Worsnop, D. R. and Laaksonen, A.: An amorphous solid state of biogenic secondary organic aerosol particles, Nature, 467(7317), 824–827, doi:10.1038/nature09455, 2010.

Wilson, J., Imre, D., Berack, J., Shrivastava, M. and Zelenyuk, A.: Evaporation Kinetics of Laboratory-Generated Secondary Organic Aerosols at Elevated Relative Humidity, , doi:10.1021/es505331d, 2015.

Yli-Juuti, T., Pajunoja, A., Tikkanen, O.-P., Buchholz, A., Faiola, C., Väisänen, O., Hao, L., Kari, E., Peräkylä, O., Garmash, O., Shiraiwa, M., Ehn, M., Lehtinen, K. and Virtanen, A.: Factors controlling the evaporation of secondary organic aerosol from α-pinene ozonolysis, Geophys. Res. Lett., 44(5), 2016GL072364, doi:10.1002/2016GL072364, 2017.

Zuend, A., Marcolli, C., Luo, B. P. and Peter, T.: A thermodynamic model of mixed organic-inorganic aerosols to predict activity coefficients, Atmospheric Chem. Phys., 8(16), 4559–4593, doi:https://doi.org/10.5194/acp-8-4559-2008, 2008.

805 Zuend, A., Marcolli, C., Booth, A. M., Lienhard, D. M., Soonsin, V., Krieger, U. K., Topping, D. O., McFiggans, G., Peter, T. and Seinfeld, J. H.: New and extended parameterization of the thermodynamic model AIOMFAC: calculation of activity coefficients for organic-inorganic mixtures containing carboxyl, hydroxyl, carbonyl, ether, ester, alkenyl, alkyl, and aromatic functional groups, Atmospheric Chem. Phys., 11(17), 9155–9206, doi:https://doi.org/10.5194/acp-11-9155-2011, 2011.

810 **Table 1**: Characteristics for the artificial data sets. Properties from top to bottom are number of VBS compounds (bins), particle diameter at the start of the evaporation, saturation concentrations of the VBS compounds and dry mole fraction of the compounds at the start of the evaporation. For C_{sat} and $X_{mole,dry}$ "Fitted" means that the parameter value was used as fitting parameter and the value was constrained between the reported minimum and maximum values.

Variable	Data set 1	Data set 2	Data set 3	Data set 4
# compounds	3	3	6	40
d_{p0} (nm)	80	10000	80	80
$C_{sat,i}$ ($\mu g\ m^{-3}$)	Fitted (min: 0.001 max: 10^4)	Fitted (min: 1 max: 10^9)	{0.001; 0.01; 0.1; 1; 10; 100}	{0.001; 0.01; 0.1; 1; 10; 100}
$X_{mole,dry}$ (t = 0 s)	Fitted (min: 0.01 max: 1)	Fitted (min: 0.01 max: 1)	Fitted (min: 0.01 max: 1)	Fitted (min: 0.01 max: 1)

815 **Table 2:** The ambient conditions and properties of the organic compounds in the artificial test data that are the same for all compounds in artificial data sets 1-4. The variables are, from top to bottom, temperature, relative humidity, gas phase diffusion coefficient, molar mass, particle phase density of the pure compound , particle surface tension and mass accommodation coefficient

Variable	Value
T (K)	298
RH (%)	80
D^a_{gas} ($cm^2 s^{-1}$)	0.05
M (g mol^{-1})	200
ρ (kg m^{-3})	1200
σ (mN m^{-1})	40
α	1

a) The gas phase diffusion coefficients are scaled to correct temperatures by multiplying with a factor of $(T/273.15)^{1.75}$ (Reid
820   et al., 1987)

Table 3: The correct parameters that are fitted in the optimization process for every artificial data sets. The order of the mole fractions is from the least volatile to the most volatile compound for artificial data sets 3 and 4

Artificial Data set	Parameter 1	Parameter 2	Parameter 3	Parameter 4	Parameter 5	Parameter 6
1	$C_{sat,1} =$ 10^{-2} µg m^{-3}	$C_{sat,2} =$ 10^{0} µg m^{-3}	$C_{sat,3} =$ 10^{3} µg m^{-3}	$X_{mole,1} = 0.5$	$X_{mole,2} = 0.4$	$X_{mole,3} = 0.1$
2	$C_{sat,1} =$ 10^{0} µg m^{-3}	$C_{sat,2} =$ 10^{3} µg m^{-3}	$C_{sat,3} =$ 10^{6} µg m^{-3}	$X_{mole,1} = 0.35$	$X_{mole,2} = 0.45$	$X_{mole,3} = 0.2$
3	$X_{mole,1} = 0.15$	$X_{mole,2} = 0.2$	$X_{mole,3} = 0.25$	$X_{mole,1} = 0.2$	$X_{mole,2} = 0.15$	$X_{mole,3} = 0.05$
4[a]	$X_{mole,1} = 0.434$	$X_{mole,2} = 0.146$	$X_{mole,3} = 0.116$	$X_{mole,4} = 0.143$	$X_{mole,5} = 0.069$	$X_{mole,6} = 0.092$

[a] The mole fractions are lumped to six volatility classes. See Table S2 for the exact values

Table 43: Composition of the mixtures 1-4 in EDB measurements and the literature values for the saturation vapor pressures.

	Component	X_{mole}	Saturation concentration C_{sat} ($\mu g\ m^{-3}$)
Mixture 1	Carbitol (2-(2-Ethoxyethoxy)ethanol)	0.39	$5.5 \cdot 10^5$ (293 K)[a]
	Glycerol	0.40	370 (293 K)[b]
	PEG$_{400}$ ($C_{2n}H_{4n}+2O_{n+1}$, n = 8.2 to 9.1)	0.21	0.0090-0.27 (298 K)[c]
Mixture 2	Carbitol (2-(2-Ethoxyethoxy)ethanol)	0.40	$5.5 \cdot 10^5$ (293 K)[a]
	Malonic acid	0.39	4 - 40 (298 K)[d]
	PEG$_{400}$ ($C_{2n}H_{4n}+2O_{n+1}$, n = 8.2 to 9.1)	0.21	0.0090-0.27 (298 K)[d]
Mixture 3	Sucrose	0.50	/
	Glycerol	0.50	370 (293K)[b]
Mixture 4	Sucrose	0.24	/
	Glycerol	0.76	370 (293K)[b]

830   [a] Data from unpublished EDB measurements, same experimental approach as in Krieger et al. (2018)

[b] Saturation concentration of glycerol at 298K from Haynes (2009) was converted to 293K using the Clasius-Clapeyron equation. The enthalpy of vaporization at boiling point (T = 562 K) was taken from Rumble et al. (2018) and corrected to 298K using equation 7-12-1 from Reid et al. (1987) resulting to ΔH_{vap} = 78.4 kJ mol^{-1}

[c] Krieger et al. (2018)

835   [d] Bilde et al. (2015)

Table 54: The properties of the organic compounds for the particles generated from mixtures 1-4. The variables are, from top to bottom, particle diameter at the start of the evaporation, molar mass, particle phase density, gas phase diffusion coefficient, relative humidity, temperature, saturation concentrations of the VBS compounds, mole fraction of the compounds at the start of the evaporation and viscosity parameters b in equation (1).

840

Variable	Mixture 1	Mixture 2	Mixture 3	Mixture 4
d_{p0} (μm)	24.29	23.70	{16.05[+];19.42[+]}	{19.02[+];24.87[+]}
M^a (g mol^{-1})	{134[d]; 92[d]; 400[e]}	{134; 104[d]; 400}	{342[d]; 92}	{342; 92}
ρ^a (kg m^{-3})	{990[d]; 1260[d]; 1130[g]}	{990; 1620; 1130}	{1580[d]; 1260}	{1580; 1260}
D^b_{gas} (cm^2 s^{-1})	{0.05;0.05;0.05}	{0.05;0.05;0.05}	{0.04; 0.09}[f]	{0.04; 0.09}[f]
RH (%)	0	0	{25; 70}	{25.1; 86.5}
T (K)	293	293	293	293
C_{sat}	Fitted	Fitted	Fitted	Fitted
	(min: 0.1 max: 10^8)	(min: 0.1 max: 10^8)	(min 1: max: 10^5)	(min: 1 max: 10^5)
$X_{mole,dry}$	Fitted	Fitted	Fitted	Fitted
(t = 0 s)	(min: 0.01 max: 1)	(min: 0.01 max: 1)	(min: 0.01 max: 1)	(min: 0.01 max: 1)
b_i^c	-	-	Fitted	Fitted
			(min: 10^{-15} max: 10^{20})	(min: 10^{-15} max: 10^{20})

+) first value is for measurement at low RH and second for measurement at high RH

a) For mixtures 1 and 2 only for the optimization runs where exact compound properties were used. The order of the compounds is the same as in the Ttable 43.

b) The order of the compounds is the same as in Ttable 43. The gas phase diffusion coefficients are scaled to

845 correct temperatures by multiplying with a factor of $(T/273.15)^{1.75}$

c) only for low RH

d) Rumble et al. (2018)

e) Mean molar mass from Krieger et al. (2018)

f) Calculated using data and equation 11-3-2 from Reid et al. (1987)

850 g) Sigma-Aldrich

Table 65: The median b-parameter which describes the contribution of glycerol and sucrose to the particle viscosity from optimizing the KM-GAP model to match the low RH measurement of mixtures 3 and 4.The literature values for viscosity of glycerol is also reported. For sucrose the reported literature value is an experimental fit calculated from viscosity measurements of sucrose-water mixtures evaluated at RH=0%.

	$\log_{10}(b_i)$ median	$\log_{10}(b_i)$ 10th / 90th percentile	$\log_{10}(\eta_i)$ literature (Pa s)
Mixture 3: glycerol	-5.1	-12.0 / -0.2	-0.030[a]
Mixture 4: glycerol	-6.5	-11.3 / -3.3	-0.030[a]
Mixture 3: Sucrose	12.8	9.6 / 16.5	15.92 ± 1.92[b]
Mixture 4: Sucrose	12.3	10.9 / 15.6	15.92 ± 1.92[b]

a) Rumble et al., (2018) b) Song et al. (2016)
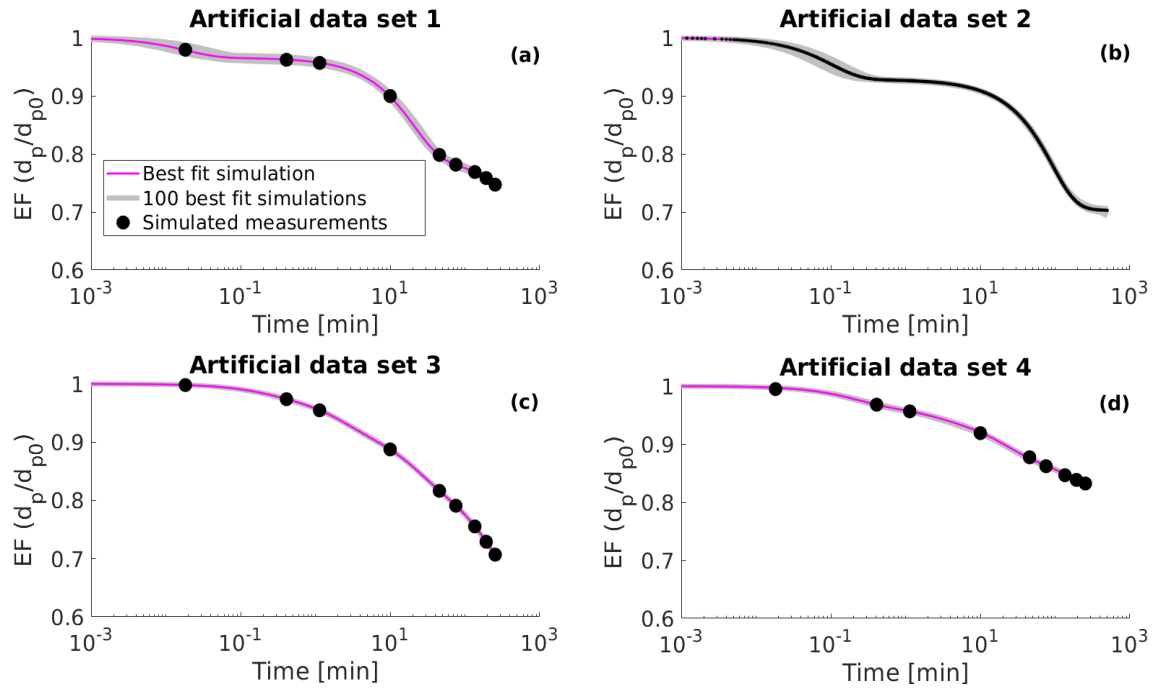
Figure 1: Simulated evaporation factors (EF, particle diameter d_p divided by the initial diameter d_{p0}) (black circles), 100 best fit simulations (grey lines) and the best fit simulation (magenta line) for a) artificial data set 1, b) artificial data set 2, c) artificial data set 3, d) artificial data set 4. The best fit simulation is determined as the evaporation simulation that produces smallest mean squared error relative to the measurement data.
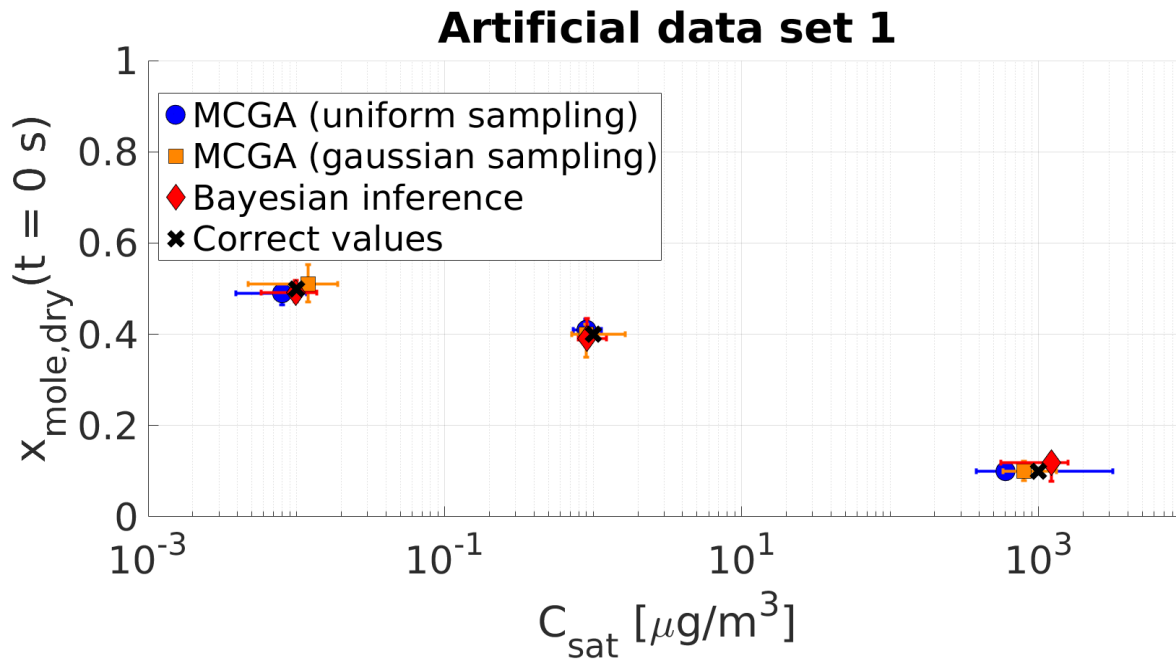
Figure 2: a) Parameter estimates from the three different optimization methods applied to artificial data set 1. Shown are MCGA with uniform sampling (blue circles), MCGA with sampling distributions similar to the Bayesian inference (Gaussian sampling, yellow squares) and Bayesian inference (red diamonds). The markers show the modes of the estimated variable distributions for MCGA methods and the maximum a posteriori estimate of the fitting variable distributions for the Bayesian inference. The whiskers show the 10th and 90th percentiles of the variable distributions for the MCGA methods and 90% credible interval for the Bayesian inference. b) The artificial data points which are the target of the optimization process and ten best fit simulations calculated with the LLEVAP model using the estimates from the MCGA optimization with uniform sampling.
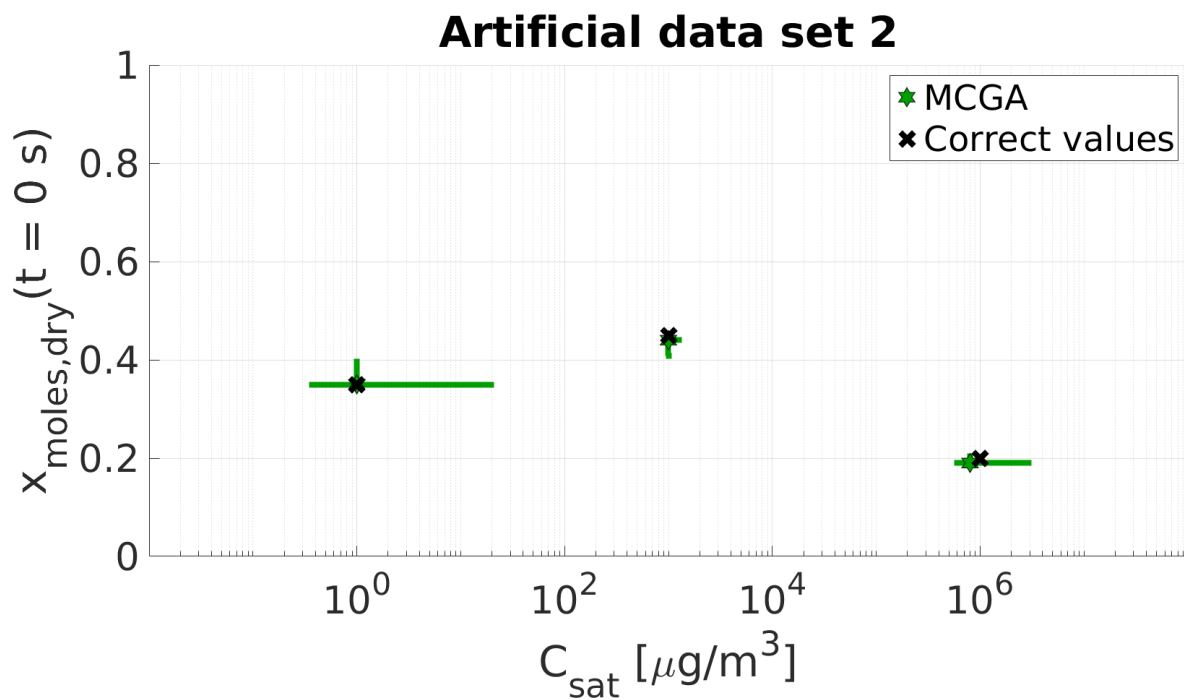
Figure 3: Parameter estimates for artificial data set 2; dry particle mole fraction at the start of the evaporation and saturation concentrations of three model compounds were optimized to match the data. Green stars show the MCGA estimates and black crosses the correct values. The whiskers show the 10th and 90th percentiles of the estimated variable distributions.
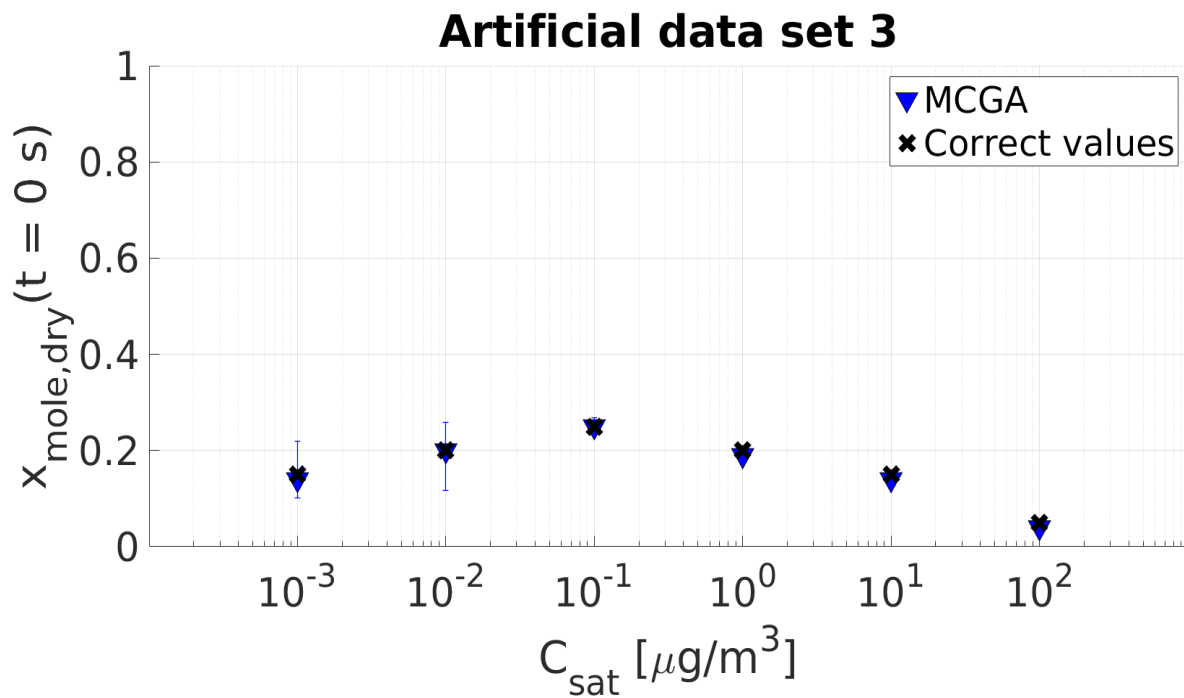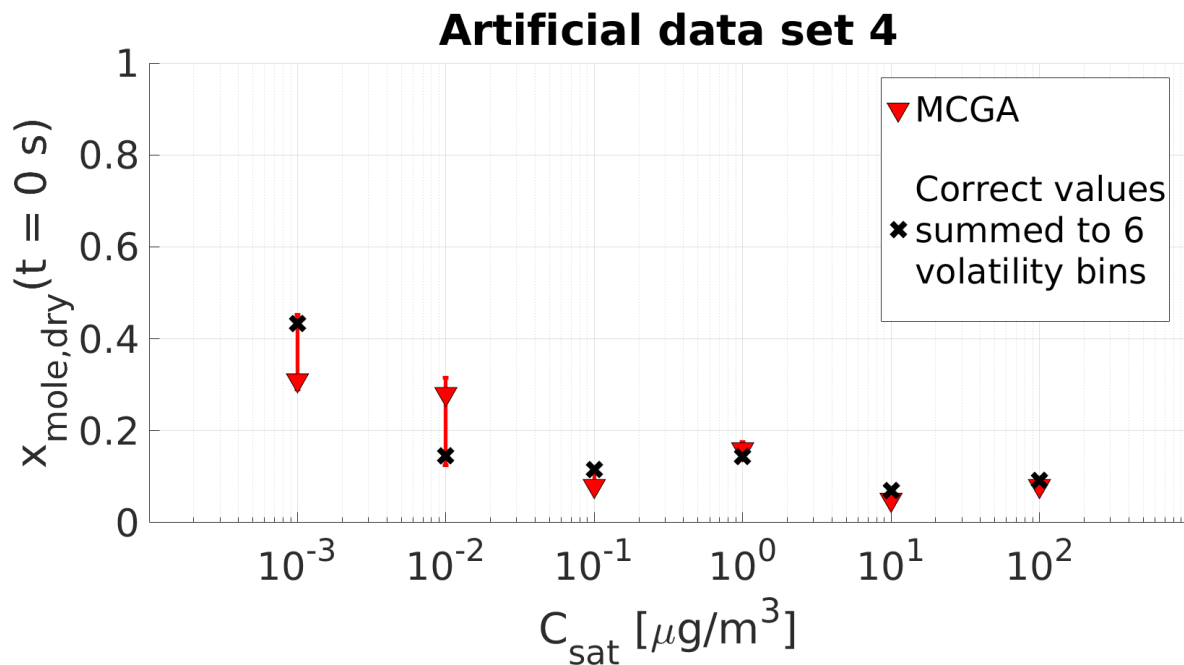
Figure 4: Parameter estimates for artificial data set 3; dry particle mole fraction at the start of the evaporation of six model compounds with predefined saturation concentration were optimized to match the data. Blue triangles show the MCGA estimates and black crosses the correct values. The whiskers show the 10th and 90th percentiles of the estimated variable distributions.

Figure 5: Parameter estimates for artificial data set 4; dry particle mole fraction at the start of the evaporation of six model compounds with predefined saturation concentration were optimized to match the data. Red triangles show the MCGA estimates and the whiskers show the 10th and 90th percentiles of the estimated variable distributions. Black crosses are the correct values summed to 6 volatility bins. All the correct values for the 40 evaporating compounds are listed in Table S2₊.
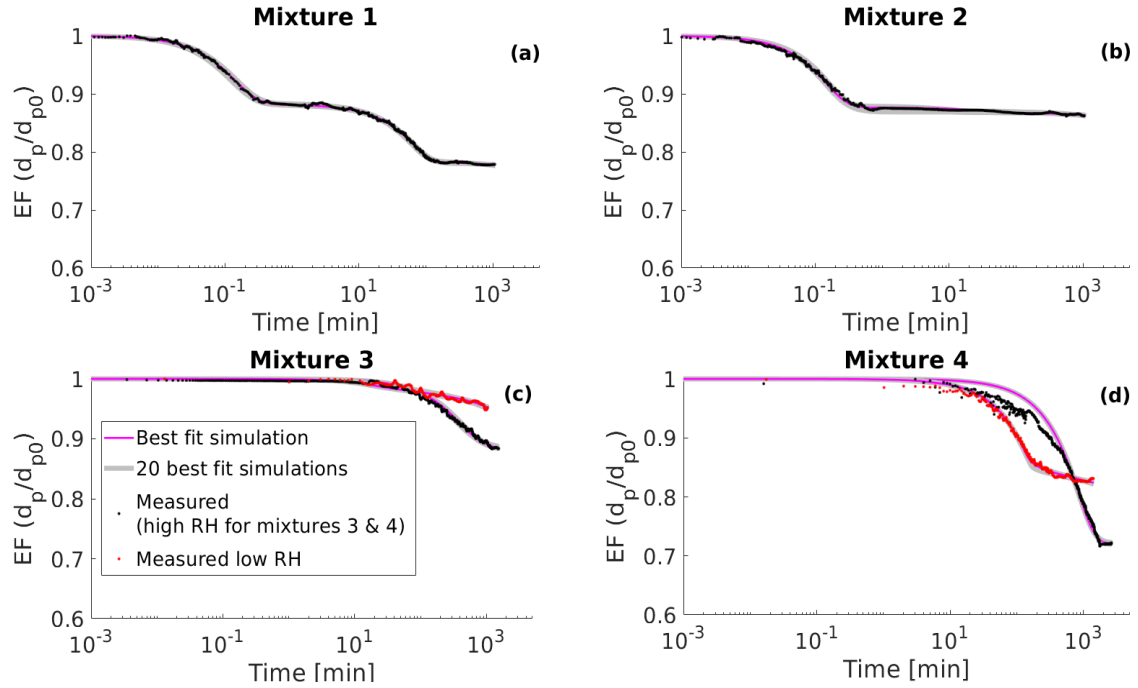
Figure 6: a) Measured evaporation factors (EF, particle diameter d_p divided by the initial diameter d_{p0}) of mixture 1 from the determined point of water equilibrium (see Sect. 5) (black circles), 20 best fit simulations (grey lines) and the best fit simulation (magenta line). b) Same as (a) but for mixture 2. c) Measured evaporation factors of mixture 3 from the determined point of water equilibrium under high RH conditions (RH=70%, black circles) and low RH conditions (RH=25%, red circles), Grey lines show 20 best fit simulations and magenta line the best fit simulation d) same as (c) but for mixture 4 for which the high RH is 86.5% and low RH is 25.1%. The best fit simulation is determined as the evaporation simulation that produces smallest mean squared error relative to the measurement data.
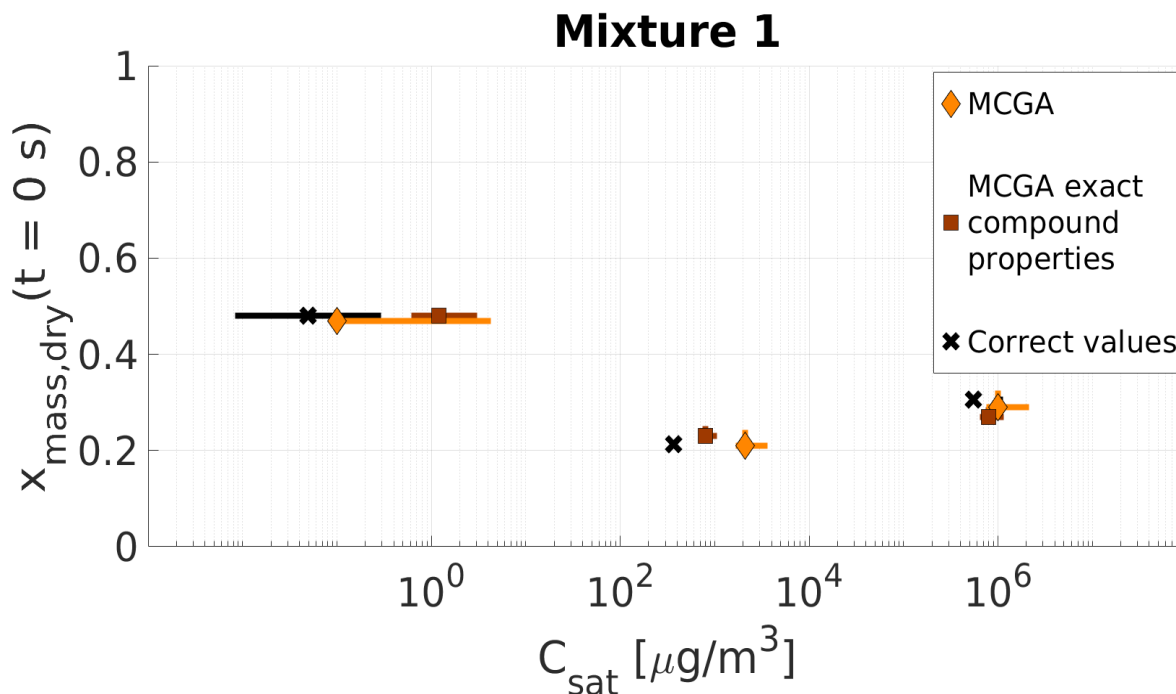
Figure 7: a) Parameter estimates for particles generated from mixture 1. Dry particle mass fraction at the start of the evaporation of three compounds and their saturation concentrations were optimized to match the evaporation data. Orange diamonds show the MCGA estimates calculated by assuming equal molar mass and particle phase density for all compounds and brown squares show the MCGA estimates calculated by setting the molar mass and particle phase density to their literature values. Black crosses show the ~~correct~~ literature values. The whiskers of the estimates show the 10th and 90th percentiles of the estimated variable distributions and the whiskers ~~in correct values~~ show the range of literature values (see Table ~~4~~3 for references). b) The measured evaporation curve which is the target of the optimization process and ten best fit simulated evaporation curves calculated with the LLEVAP model using the estimates from optimization.
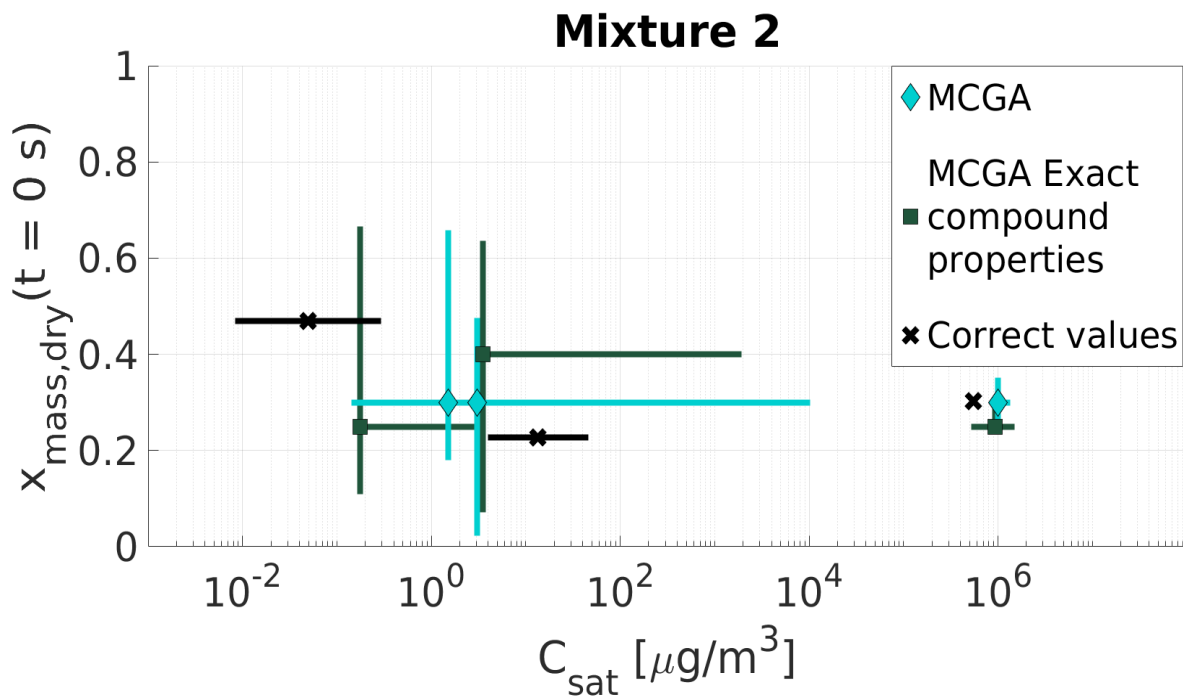
Figure 8: Parameter estimates for particles generated from mixture 2. Dry particle mass fraction at the start of the evaporation of three compounds and their saturation concentrations were optimized to match the evaporation data. Cyan diamonds show the MCGA estimates calculated by assuming equal molar mass and particle phase density for all compounds and teal squares show the MCGA estimates calculated by setting the molar mass and particle phase density to their literature values (see Table 4̶3 for references). Black crosses show the ~~correct~~ literature values. The whiskers of the estimates show the 10th and 90th percentiles of the estimated variable distributions and the whiskers ~~in correct values~~ show the range of literature values.
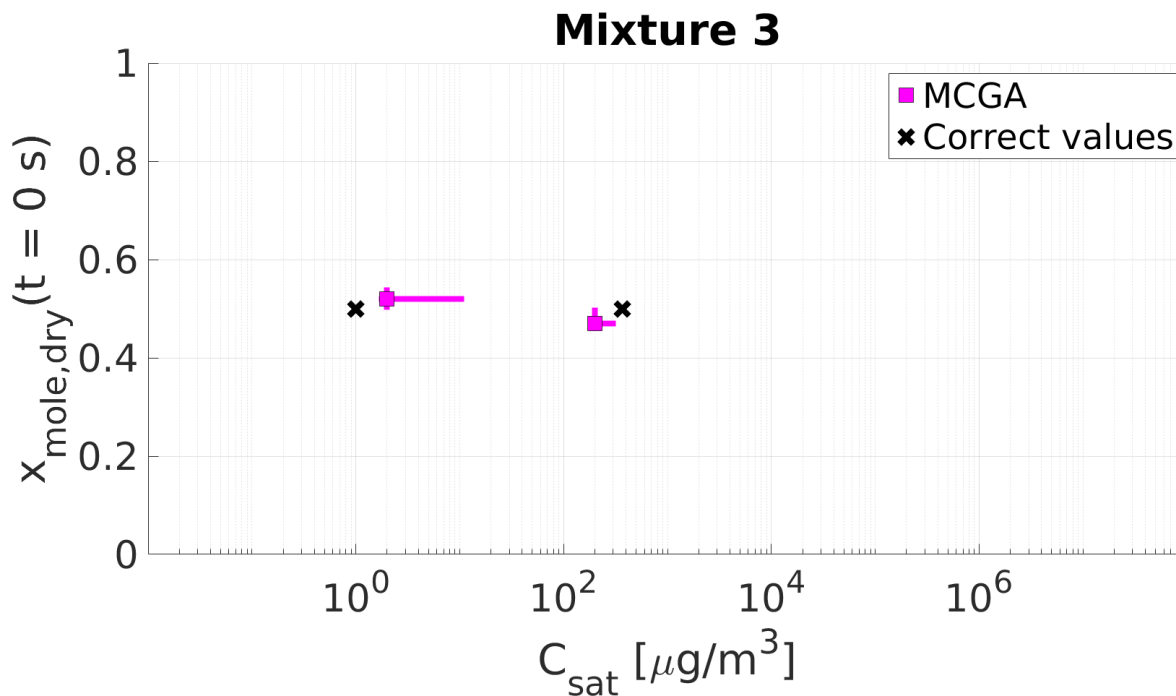
Figure 9: Parameter estimates for particles generated from mixture 3. Dry particle mole fraction at the start of the evaporation of three compounds and their saturation concentrations were optimized to match the evaporation data. Magenta squares show the MCGA estimates and black crosses show the ~~literature~~ correct values. The whiskers show the 10th and 90th percentiles of the estimated variable distributions. ~~Correct value of S~~sucrose C_{sat} is marked at the lower limit of the C_{sat} range due to its assumed low value.
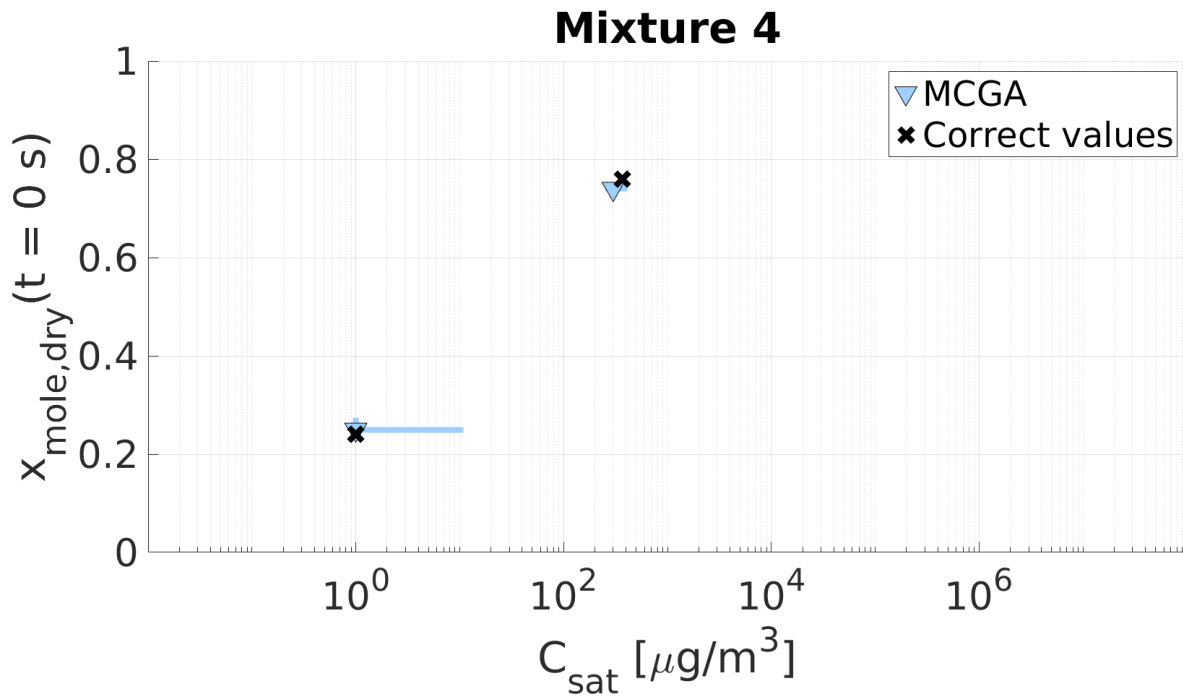
Figure 10:Parameter estimates for particles generated from mixture 4. Dry particle mole fraction at the start of the evaporation of three compounds and their saturation concentrations and the viscosity parameters b_i were optimized to match the evaporation data. Magenta squares show the MCGA estimates and black crosses show the literature ~~correct~~ values. The whiskers show the 10th and 90th percentiles of the estimated variable distributions. ~~Correct value of s~~Sucrose C_{sat} is marked at the lower limit of the C_{sat} range due to its assumed low value.